Dalton Transactions

ROYAL SOCIETY OF CHEMISTRY

PERSPECTIVE

View Article Online
View Journal | View Issue

Cite this: *Dalton Trans.*, 2026, **55**, 4015

Aliovalent solid solutions of metal–organic frameworks

Marco Taddei

Received 18th November 2025,
Accepted 18th January 2026

DOI: 10.1039/d5dt02764k

rsc.li/dalton

Metal–organic frameworks (MOFs) are amenable to the formation of solid solutions by the isomorphous substitution of the organic linker and/or the metal ion. In the case of metal substitution, the incorporation of aliovalent species, *i.e.*, species having a different oxidation state than the original ion, leads to the generation of excess charges in the framework, which must be compensated. Depending on the charge compensation mechanism, new properties can emerge. Although limited work has been done so far in this research area, aliovalent substitution has the potential to become an important tool to fine-tune the physico-chemical properties of MOFs and should be investigated more systematically. Here, the available literature on the aliovalent solid solutions of MOFs is critically analysed under the lens of inorganic solid-state chemistry.

Introduction

Substitutional solid solutions are commonplace in inorganic solid-state chemistry.[1,2] The primary requirement to achieve substitution in an inorganic compound is that the substituent should be isomorphic with the original element, *i.e.*, that they have similar atomic/ionic radii and can adopt the same coordination geometry. Substitutional solid solutions can be either *isovalent*, if the substituent has the same oxidation state as that of the original element, or *aliovalent*, if the oxidation states are different. Upon introduction of an aliovalent species to the crystal structure, excess negative or positive charges are created, depending on whether the aliovalent ion has a lower (*subvalent*) or higher (*supervalent*) oxidation state than the original ion. The ways in which excess charges are compensated can vary depending on the crystal structure: the presence of a supervalent substituent can be compensated either by interstitial/extraframework anions or by cation vacancies; the presence of a subvalent substituent can be compensated either by interstitial/extraframework cations or by anion vacancies. As a consequence of the charge compensation mechanism, aliovalent substitution leads to the emergence of new properties.

Notable examples of aliovalent solid solutions of practical interest include zeolites (porous aluminosilicates), layered double hydroxides (LDHs) and doped fluorite-type tetravalent metal (M^{IV}) oxides (Fig. 1).

In zeolites (Fig. 1a), the presence of subvalent Al^{III} in the tetrahedral sites of a porous $Si^{IV}O_2$ matrix creates negative charges on the framework.[3] These charges are compensated by extraframework cations accommodated within the cages of the zeolitic framework. Being crystalline and microporous, zeolites are widely used in industry as cation exchangers[4] and adsorbents for small molecules.[5] By tuning the Si/Al ratio, the ion-exchange capacity, acid/base stability, and hydrophilicity can be adjusted. Post-synthesis treatment such as annealing of the ammonium-exchanged form creates Brønsted and/or Lewis acidic sites.[6] This has huge relevance for acid-catalysed industrial processes, such as fluid catalytic cracking, where ultrastable zeolite Y is the state-of-the-art catalyst.[7] Similarly, the substitution of tetrahedral Si^{IV} for P^{V} in zeolite-like aluminium phosphates makes the framework negatively charged with analogous implications.[3]

In hydrotalcite, a naturally occurring LDH (Fig. 1b), the introduction of supervalent Al^{III} in brucite-type layers [brucite is $Mg(OH)_2$] made up of edge-sharing [$Mg^{II}(OH)_6$] octahedra, creates excess positive charges on the layers.[8] These charges are compensated by the intercalation of anionic species in the interlayer space (carbonate in the case of natural hydrotalcite). LDHs can be prepared by combining a range of divalent cations (M^{II}: Mg^{II}, Co^{II}, Ni^{II}, Cu^{II}, and Zn^{II}) and trivalent cations (M^{III}: Al^{III}, Cr^{III}, Fe^{III}, and Ga^{III}) and are widely used as anion exchangers, basic catalysts, and drug delivery platforms.[9,10] By varying the M^{II}/M^{III} ratio, the charge density on the LDH layers can be adjusted, influencing the ion-exchange behaviour and capacity. Besides common inorganic anions, such as CO_3^{2-}, Cl^- and NO_3^-, LDHs have been used as hosts for a wide range of anionic species, including pharmaceutically active molecules,[11] DNA strands[12] and organometallic complexes.[13,14]

Department of Chemistry and Industrial Chemistry, INSTM Research Unit, University of Pisa, Via G. Moruzzi 13, 56124 Pisa, Italy. E-mail: marco.taddei@unipi.it

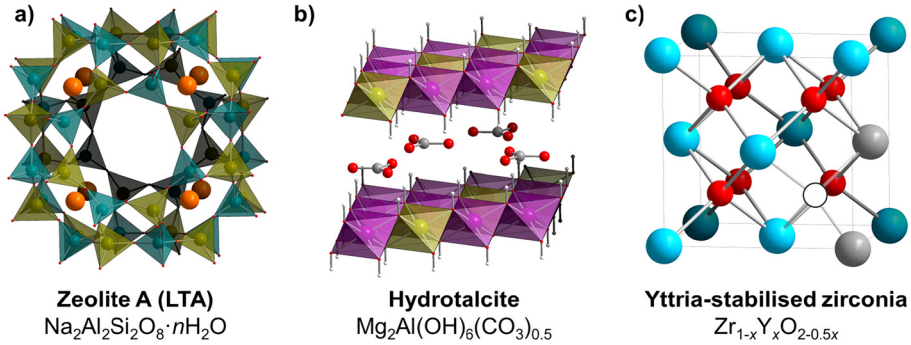

Fig. 1 Polyhedral representation of the α-cage found in zeolite A, showing the ordered arrangement of Si^{IV} (teal) and Al^{III} (dark yellow) over tetrahedral sites within the framework and the location of extraframework Na^+ ions (orange) within the cage (a). Polyhedral representation of hydrotalcite, showing the arrangement of Mg^{II} (violet) and Al^{III} within the layers and the location of CO_3^{2-} ions (C, grey; O, red) in the interlayer space (b). Unit cell of cubic yttria-stabilised zirconia, where two Y^{III} (grey) substitute two Zr^{IV} (light blue), generating an oxygen vacancy (empty circle) (c).

Among oxides, aliovalent solid solutions of fluorite-type M^{IV} oxides, *i.e.* zirconia ($Zr^{IV}O_2$) and ceria ($Ce^{IV}O_2$), have prominent technological importance as electrolytes in solid oxide fuel cells and catalysts (Fig. 1c).[15] The cubic form of zirconia (as well as hafnia [$Hf^{IV}O_2$]), displaying a fluorite-type structure with 8-coordinated Zr^{IV}, is metastable under ambient conditions, converting into the monoclinic form, which features 7-coordinated Zr^{IV}.[16] By forming aliovalent solid solutions with subvalent ions, such as Y^{III}, Sc^{III}, lanthanides (Ln^{III}), Mg^{II}, and Ca^{II}, the cubic polymorph can be stabilised under ambient conditions. Aliovalent solid solutions of ceria ($Ce^{IV}O_2$), which is thermodynamically stable under ambient conditions in a fluorite-type structure, are also known with a range of M^{III}, mainly Ln^{III}.[17] The main charge compensation mechanism in these oxides involves the generation of oxygen vacancies, which are responsible for their high oxide-ion conductivity,[15] catalytic activity[18] and giant piezoelectric effect.[19]

Solid solutions of metal–organic frameworks

Metal–organic frameworks (MOFs) are a class of crystalline and porous coordination polymers built from the connection of metal cations (or clusters thereof) and organic linkers (primarily carboxylates anions).[10] In principle, MOFs offer the unique opportunity to form solid solutions *via* isomorphous replacement of both organic linkers and metal ions.[20] Although, at least in principle, aliovalent substitution of organic linkers can be achieved (*e.g.*, through the isomorphic replacement of a linker with an analogue bearing a charged functional group on the backbone), aliovalent substitution of metal ions allows to draw parallels with inorganic materials and is the main object of interest in the present study. The concept of aliovalent substitution has, rather surprisingly, not attracted much attention so far in the MOF literature, with only 11 articles using the term "aliovalent" and only 168 using the term "solid solution" associated with "metal organic framework" out of more than 90 000 featuring the string "metal organic framework" (see Table 1).

Table 1 Number of articles published since the year 2000, which contain the given search strings in title/abstract/keywords

String	Articles	Share
"Metal organic framework"	90 592	100%
"Metal organic framework" + "bimetallic"	3549	3.9%
"Metal organic framework" + "mixed metal"	586	0.6%
"Metal organic framework" + "heterometallic"	481	0.5%
"Metal organic framework" + "mixed valence"	234	0.3%
"Metal organic framework" + "solid solution"	168	0.2%
"Metal organic framework" + "aliovalent"	11	0.01%

Source: scopus (retrieved on 30/06/2025).

Before delving into the literature on aliovalent substitution in MOFs, it is appropriate to spend some words regarding the terminology employed in the literature to refer to MOFs containing more than one metal species, which includes the terms "bimetallic", "heterometallic" and "mixed metal" (Table 1). Although these terms are sometimes used to refer to true solid solutions, *i.e.*, where different metals occupy the same crystallographic sites, they are also used in other instances: i. MOFs in which multiple metals constitute the inorganic unit but occupy distinct crystallographic sites and display distinct coordination environments (*e.g.*, MUV-10, based on inorganic units containing Ca^{II} in capped trigonal prismatic geometry and Ti^{IV} in octahedral geometry);[21] ii. MOFs that contain metal atoms outside of the inorganic unit (*e.g.*, CAU-30, where Zr^{IV} is part of the inorganic unit and Ni^{II} is coordinated within the porphyrinic rings of the linker);[22] iii. core-shell structures constitute phase-pure domains (derived from either concentration gradients due to diffusional limitations during post-synthetic exchange[23] or crystallisation occurring with different kinetics depending on the metal species).[24] All of these instances do not classify as solid solutions and are, therefore, not of interest for this perspective.

Isovalent metal substitution in MOFs has been the main object of interest to date.[25–27] This has provided mixed metal

analogues of some prominent MOF topologies, such as M^{II}-based MOF-5,[28,29] HKUST-1[23,30,31] and MOF-74,[32–34] M^{III}-based MIL-53[24,35] and MIL-100/101,[36,37] and M^{IV}-based UiO-66, MOF-808 and other frameworks based on the same hexanuclear oxoclusters.[38–40] Aliovalent substitution has attracted less attention, likely because of the synthetic challenge of identifying the appropriate reaction conditions to embed two metals with different oxidation states in the same crystallographic sites within the inorganic building unit. Aside from different charge-neutrality requirements, metals with different oxidation states are likely to have different ionic radii and/or preferred coordination geometries that are not compatible with their incorporation in the same inorganic building units, leading to limited solid solubility. Furthermore, the different hardness levels of metal ions with different charges affect the metal–ligand affinity, so that selective crystallisation may take place during synthesis, potentially resulting in the segregation of homometallic phases. For this reason, post-synthetic approaches have often been used to achieve aliovalent substitution in MOFs.[41]

In the following sections, existing literature on aliovalent substitution in MOFs is critically analysed under the lens of inorganic solid-state chemistry. MOFs are grouped into subclasses based on the oxidation state of the original metal, and emphasis is given to the demonstration of the effective formation of the solid solution and to the clarification of the nature of the charge compensation mechanism. Given the central role of the ionic radius (r) in enabling isomorphic substitution, the values of r according to Shannon[42] for the given coordination numbers (CNs) for the species relevant to this discussion are provided in Table 2.

Aliovalent metal substitution in MOFs

M^{II}-MOFs

M^{II}-MOFs (M^{II} = Mg^{II}, Ca^{II}, Mn^{II}, Co^{II}, Ni^{II}, Cu^{II}, Zn^{II}, Cd^{II}, and Pb^{II}) commonly feature CNs comprised between 4 and 6, although CNs as high as 8 can be observed for species with larger r (Ca^{II}, Cd^{II}, Pb^{II}). These MOFs reportedly undergo aliovalent substitution with either M^{I}, M^{III} or M^{IV}. The introduction of subvalent M^{I} generates an excess negative charge, which is reportedly compensated by the loss of a terminal coordinating anion, such as chloride. The introduction of supervalent M^{III} or M^{IV} results in frameworks with an excess positive charge, which is usually compensated by the inclusion of anions, rather than by the generation of metal cation vacancies. As an alternative to the removal/addition of anionic ligands, protonation/deprotonation of oxide species, hydroxide groups or coordinated water molecules, if present in the inorganic unit, could also represent a means to compensate excess negative/positive charge, although these compensation mechanisms have seldom been observed to date.

The earliest report on aliovalent substitution in MOFs is perhaps a study on the post-synthetic ion metathesis in a MOF with the formula $Cd_{1.5}(H_3O)_3[(Cd_4O)_3(hett)_8(CH_3OH)_4]$ (where $hett^{3-}$ is 5,5′,10,10′,15,15′-hexaethyltruxene-2,7,12-tricarboxylate), featuring 8-coordinated Cd^{II}, which dates back to 2009.[43] The framework is negatively charged, requiring extraframework Cd^{2+} and H_3O^+ ions for charge neutrality. The authors successfully replaced Cd^{II} with Dy^{III} and Nd^{III} by soaking single crystals of the parent MOF in a methanolic solution of the respective nitrate salts, obtaining fully exchanged, monometallic analogues not accessible *via* direct synthesis. Single-crystal X-ray diffraction (SCXRD) analysis of the Dy-based compound revealed that the $[Cd_4(\mu_4\text{-}O)(R\text{-}COO)_8(CH_3OH)_4]^{2-}$ secondary building units (SBUs) in the parent MOF were transformed into $[Dy_4(\mu_2\text{-}OH)(R\text{-}COO)_8(CH_3OH)_4]^{3+}$ units (Fig. 2), thereby generating an excess positive charge compensated by the presence of extraframework nitrate anions to afford a MOF with the formula $[(Dy_4OH)_3(hett)_8(CH_3OH)_{12}]\cdot 9NO_3$. Dy^{III} was 7- or 8-coordinated, depending on the binding with the central μ_2-OH group. Thus, a potential cation exchanger was turned into a potential anion exchanger, although the ion-exchange properties of these MOFs were not investigated. Partially exchanged compounds were obtained at shorter contact times

Table 2 Ionic radii (r) of relevant species. LS = low spin; HS = high spin; and SQ = square planar

Species	CN	r (Å)	Species	CN	r (Å)	Species	CN	r (Å)
Li^{I}	4	0.59	Fe^{II}	6	0.61 (LS)	Zr^{IV}	6	0.72
Mg^{II}	6	0.72			0.78 (HS)		8	0.84
	8	0.89	Fe^{III}	6	0.55 (LS)	Cd^{II}	6	0.95
Al^{III}	6	0.535			0.645 (HS)		8	1.1
Ca^{II}	7	1.06	Co^{II}	6	0.65 (LS)	In^{III}	6	0.8
Sc^{III}	6	0.745			0.745 (HS)		8	0.92
Ti^{III}	6	0.67	Ni^{II}	4SQ	0.49	La^{III}	6	1.032
Ti^{IV}	6	0.605		6	0.69	Ce^{III}	6	1.01
V^{III}	6	0.64	Cu^{I}	4	0.6		8	1.143
V^{IV}	6	0.58		6	0.77	Ce^{IV}	8	0.97
V^{V}	6	0.54	Cu^{II}	5	0.65	Pr^{III}	6	0.99
Cr^{II}	6	0.73 (LS)		6	0.73	Nd^{III}	8	1.109
		0.8 (HS)	Zn^{II}	4	0.6	Sm^{III}	6	0.958
Cr^{III}	6	0.615		6	0.74	Tb^{III}	6	0.923
Mn^{II}	6	0.67 (LS)	Ga^{III}	6	0.62	Dy^{III}	8	1.027
		0.83 (HS)	Y^{III}	6	0.9			

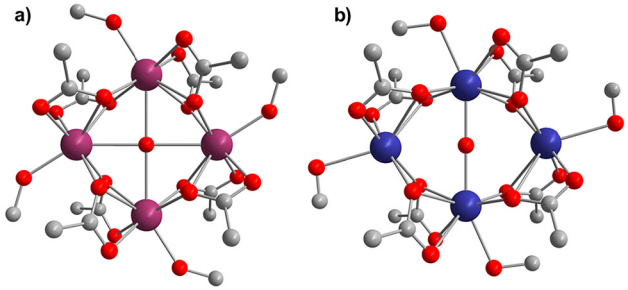

Fig. 2 Structures of the $[Cd_4(\mu_4\text{-}O)(R\text{-}COO)_8(CH_3OH)_4]^{2-}$ (a) and $[Dy_4(\mu_2\text{-}OH)(R\text{-}COO)_8(CH_3OH)_4]^{3+}$ (b) SBUs. The Dy atoms in (b) are disordered over two sites with 0.5 occupancy each; only half of them are represented for the sake of clarity to highlight the 7- and 8-coordinated environments. Colour code: Cd, purple; Dy, blue; C, grey; and O, red.

of the parent MOF with the lanthanide nitrate solution; however, they were not investigated further either. Given the tolerance of the framework to the complete replacement of Cd^{II}, one might reasonably expect that the partially exchanged compounds are aliovalent solid solutions; however, it cannot be excluded that Dy^{III} and Cd^{II} segregate into homometallic SBUs that might even coexist within the same crystalline domains.

Subsequently, the same authors attempted to post-synthetically exchange Fe^{II} for Mn^{II} in single crystals of POST-65(Mn), a MOF with a similar structure to the above-described Cd-based MOF and formula $Mn(H_3O)[(Mn_4Cl)_3(hmtt)_8(DMF)_{12}]$ (where $hmtt^{3-}$ is 5,5′,10,10′,15,15′-hexamethyltruxene-2,7,12-tricarboxylate and DMF is *N*,*N*-dimethylformamide).[44] POST-65 (Mn) features negatively charged $[Mn_4(\mu_4\text{-}Cl)(R\text{-}COO)_8(DMF)_4]^-$ SBUs with 6-coordinated Mn^{II} (Fig. 3a) and extraframework Mn^{2+} and H_3O^+ species for charge balance. Complete Mn^{II} exchange was achieved when the MOF was soaked in a $FeCl_2$ solution, which led to the incorporation of Fe^{III} to yield a MOF featuring negatively charged $[Fe_4(\mu_4\text{-}OH)(\mu_2\text{-}O)_2(R\text{-}COO)_8]^-$ SBUs, where two additional oxo bridges are present to compensate the excess positive charge carried by Fe^{III}, whose average CN is 5.5 (Fig. 3b). The MOF was formulated as Fe $[(Fe_4OH)_3O_6(hmtt)_8]$, with one extraframework Fe^{3+} for overall charge balance. The oxidation state of Fe was confirmed *via* X-ray absorption near-edge spectroscopy (XANES) at the Fe K-edge. Given the different chemical compositions of the SBUs, the formation of aliovalent solid solutions upon partial exchange is not obvious in this case, but the authors did not delve further into this issue.

A similar post-synthetic ion metathesis approach was applied to MOF-5 with the formula $Zn_4O(BDC)_6$ (where BDC^{2-} is 1,4-benzenedicarboxylate), featuring 4-coordinated Zn^{II} assembled into $[Zn_4(\mu_4\text{-}O)(R\text{-}COO)_6]$ SBUs (Fig. 4).[29] In this study, Zn^{II} was exchanged with both a range of M^{II} and with Ti^{III}, V^{III} and Cr^{III}. The formation of the solid solution was presumed based on the evidence of a single crystalline phase in the powder X-ray diffraction (PXRD) patterns, and chemical analysis revealed the presence of stoichiometric chloride in M^{III}-substituted MOF-5 as a means to compensate the excess positive charge. Evidence of the incorporation of M^{III} in the SBUs of MOF-5 was provided by UV-Visible and electron paramagnetic resonance (EPR) spectroscopies. This led to the proposal of the general formula $[Zn_{4-x}M^{III}_xCl_x(\mu_4\text{-}O)(R\text{-}COO)_6]$, where x = 0.09 for M^{III}═Ti^{III}, 0.20 for M^{III}═V^{III} and 1.41 for M^{III}═Cr^{III}. The authors explained this trend by suggesting that the degree of exchange is kinetically controlled by the stability constants of each substituting cation. The significantly higher incorporation of Cr^{III} could also be explained with its smaller r, compared with Ti^{III} and V^{III}, which could increase its solubility in the SBU. The presence of coordinated chloride leads to M^{III} defects with a CN of 5 (Fig. 4). The authors also demonstrated the possibility to exchange Cr^{II}, followed by oxidation to Cr^{III} using $NOBF_4$ in acetonitrile, leading to the formation of a MOF where BF_4^- serves as an extraframework anion to neutralise the excess positive charge.

More recently, attempts were made to post-synthetically exchange a range of M^{II} (Fe^{II}, Co^{II}, Ni^{II}, Cu^{II}, Zn^{II}) for Ca^{II} into heterobimetallic MUV-10 with the formula $Ti_3Ca_3O_2(BTC)_4(H_2O)_6$, (where BTC^{3-} is 1,3,5-benzenetricarboxylate) featuring $[Ti_2Ca_2(\mu_3\text{-}O)_2(R\text{-}COO)_8(H_2O)_4]$ SBUs with 6-coordinated Ti^{IV} and 7-coordinated Ca^{II} (Fig. 5). The exchange of Cu^{II} led to the transformation of MUV-10 into MUV-102, an aliovalent solid solution incorporating 20% of Ti^{IV} in the

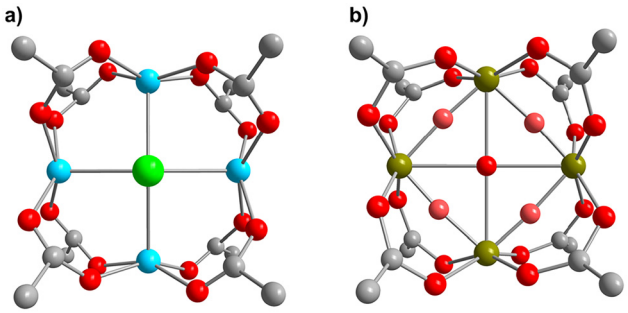

Fig. 3 Structures of the $[Mn_4(\mu_4\text{-}Cl)(R\text{-}COO)_8]^-$ (a) and $[Fe_4(\mu_4\text{-}OH)(\mu_2\text{-}O)_2(R\text{-}COO)_8]^-$ (b) SBUs. The DMF molecules in (a) were not located *via* the SCXRD analysis. The μ_2-O atoms in (b) are disordered over two sites with 0.5 occupancy each and are represented in pale red. Colour code: Mn, cyan; Fe, dark yellow; Cl, green; C, grey; and O, red.

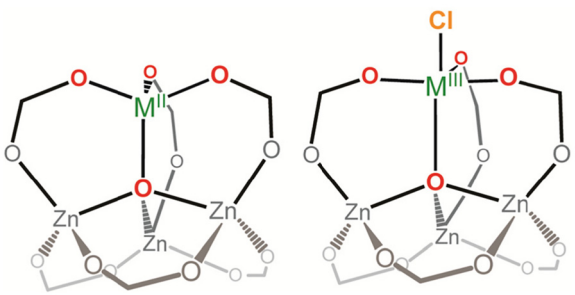

Fig. 4 Structures of the $[Zn_3M^{II}(\mu_4\text{-}O)(R\text{-}COO)_6]$ (left) and $[Zn_3M^{III}Cl(\mu_4\text{-}O)(R\text{-}COO)_6]$ SBUs with 5-coordinated M^{III} (right). Reproduced with permission from ref. 29. Copyright 2013, the American Chemical Society.

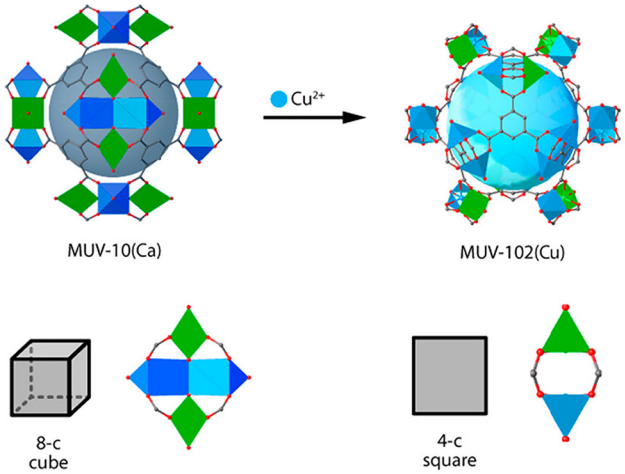

Fig. 5 Post-synthetic transformation of MUV-10, based on the 8-connected $[Ti_2Ca_2(\mu_3\text{-}O)_2(R\text{-}COO)_8(H_2O)_4]$ SBUs, into MUV-102, based on the 4-connected $[CuTi(R\text{-}COO)_4(H_2O)O]$ SBUs. Colour code: Ti, green; Ca, blue; Cu, cyan; C, grey; and O, red. Adapted with permission from ref. 45. Copyright 2020, the American Chemical Society.

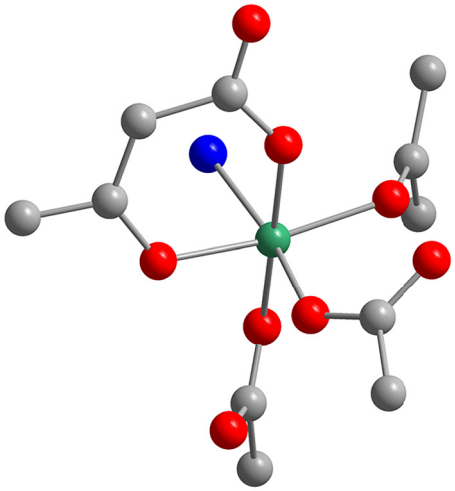

Fig. 6 Coordination environment of Ni^{II} in MOF-74. Colour code: Ni, sea green; C, grey; O, red; and H_2O, blue.

dinuclear Cu^{II}-based paddlewheel SBUs of HKUST-1 with the formula $[Cu_2(R\text{-}COO)_4(H_2O)_2]$.[45] The formation of heterometallic clusters was proved *via* extended X-ray absorption fine structure (EXAFS) spectroscopy at the Ti K-edge, which indicates the presence of Ti–Cu distances at *ca.* 2.84 Å. In addition, Ti and Cu K-edge XANES data indicated the simultaneous presence of highly distorted 6-coordinated Ti^{IV} and 5-coordinated Cu^{II} centers in MUV-102(Cu). The formation of heterometallic paddle wheel units was also consistent with the presence of uncoupled cupric $S = \frac{1}{2}$ signals in the EPR spectrum of MUV-102. The authors argued that the excess positive charge might be counterbalanced by the coordination of O^{2-} capping ligands (presumably derived from the complete deprotonation of coordinated water molecules) to Ti^{IV} in heterometallic $[CuTi(R\text{-}COO)_4(H_2O)O]$ SBUs.

MOF-74(Ni) with the formula $Ni_2(DOBDC)(H_2O)_2$ (where $DOBDC^{2-}$ is 2,5-dioxido-1,4-benzenedicarboxylate) was the object of investigation as a platform for aliovalent substitution *via* direct synthesis.[46] This MOF features monodimensional inorganic units based on 6-coordinated Ni^{II}, where one ligand is a capping water molecule that can be removed upon activation at a high temperature under vacuum, reducing the CN to 5 and generating Lewis acidic open metal sites (OMSs) (Fig. 6). A MOF with the formula $Ni_{1.6}Fe_{0.4}(DOBDC)$ was obtained using $FeCl_2$ as a source of Fe^{II}, 90% of which was oxidised to Fe^{III} upon exposure to air. Mössbauer spectroscopy was employed to confirm the presence of Fe^{III} in high-spin configuration, whose excess positive charge was compensated by chloride, as evidenced by a combination of inductively coupled plasma optical emission spectroscopy (ICP-OES), energy-dispersive X-ray spectroscopy (EDS) and X-ray photoelectron spectroscopy (XPS). Capping chloride anions replaced neutral water ligands in the coordination sphere of Fe^{III}, as suggested by the emergence of a band at 389 cm^{-1} in the infrared (IR) spectrum, which was attributed to the presence of Fe^{III}–Cl bonds. As a result, Fe^{III} centres retain the CN of 6 upon activation.

The Zn^{II}-based MOF MFU-4*l* with the formula $Zn_5Cl_4(btdd)_3$ {where $btdd^{2-}$ is bis(1*H*-1,2,3-triazolo-[4,5-*b*],[4′,5′-*i*])dibenzo-[1,4]-dioxin} was proved to be suitable for the aliovalent substitution of Zn^{II} with either Cu^{I} or Li^{I} *via* post-synthetic exchange.[47,48] The SBUs feature one central 6-coordinated Zn^{II} and four peripheral 4-coordinated Zn^{II}, held together by 1,2,3-triazolo ligands to afford scorpionate-like complexes with terminal chloride ligands binding the peripheral Zn^{II} (Fig. 7). Two Cu^{I} per SBU were introduced using a two-step approach, involving metal exchange with $CuCl_2$ in *N*,*N*-dimethyl-

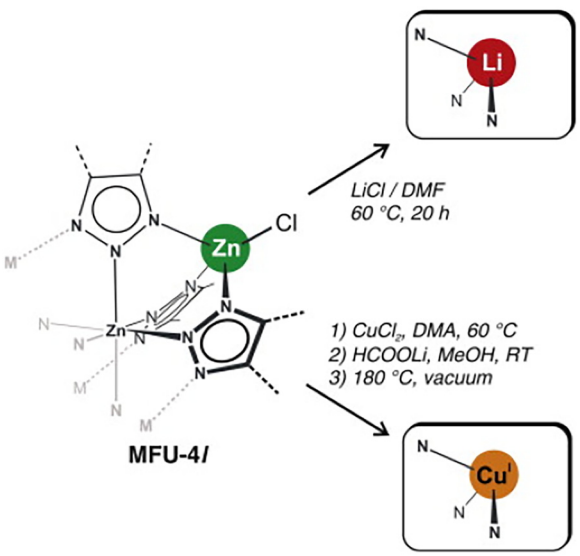

Fig. 7 Aliovalent substitution of tetrahedral Zn^{II} with Li^{I} and Cu^{I} in MFU-4*l*. Reproduced with permission from ref. 45. Copyright 2015, Elsevier.

acetamide (DMA), followed by ligand exchange with formate, which, upon thermal decomposition at 180 °C under vacuum, led to the reduction of Cu^{II} to Cu^{I}. Two Li^{I} per SBU can be exchanged by treatment with a LiCl solution in DMF. In both cases, the excess negative charge is compensated by the loss of terminal chloride ligands, leading to 3-coordinated trigonal pyramidal M^{I} and the general formula $M^{I}_2Zn_3Cl_2(btdd)_3$. The effective replacement of Zn^{II} with M^{I} was inferred *via* ICP-OES and EDS analyses, which allow to determine the M^{I}/Zn^{II} and Cl/Zn^{II} ratios. Exposure of the aliovalent exchanged MOFs to air led to filling of the coordination vacancies on Cu^{I} and Li^{I} with O_2 and H_2O, respectively. In addition, the high affinity towards the adsorption of H_2, N_2, O_2, C_2H_4 and CH_4 in Cu^{I}-MFU-4*l* clearly points to the existence of open Cu^{I} sites with π-backbonding capabilities, which are not available in the parent framework. Several follow-up studies have, in fact, explored the use of Cu^{I}-MFU-4*l* and Li-MFU-4*l* as adsorbents for hydrogen and methane storage, I_2 capture, and a number of challenging separations (H_2/D_2, O_2/N_2, N_2/CH_4, paraffin/olefin) and as catalysts for the conversion of CO_2 to CH_4.[49–62] Furthermore, the nearly complete exchange of Cr^{III} for 4-coordinated Zn^{II} was reported, leading to the inclusion of additional chloride ligands to compensate the excess positive charge and one DMF, thereby generating 6-coordinated Cr^{III} centres in a MOF with the formula $Cr_4ZnCl_8(btdd)_3(DMF)_4$.[63] The removal of DMF generates a Lewis acidic site that makes the MOF an active catalyst for the gas-phase polymerisation of ethylene.

M^{III}-MOFs

M^{III}-MOFs (M^{III} = Al^{III}, Sc^{III}, Cr^{III}, Fe^{III}, Ga^{III}, and In^{III}) commonly feature a CN of 6 and have been shown to undergo aliovalent substitution with M^{II} and M^{IV}. The inclusion of subvalent M^{II} yields a framework with an excess negative charge, which is preferentially compensated by the protonation of O/OH groups coordinated to the inorganic unit, rather than by the generation of anion vacancies, which would entail a reduction in the CN to below 6 and a consequential structural destabilisation of the inorganic unit, thereby limiting the extent of aliovalent substitution. The inclusion of supervalent M^{IV} yields a framework with an excess positive charge, which can be compensated by the deprotonation of OH/H_2O groups coordinated to the inorganic unit.

The most relevant study in the area of aliovalent substitution in MOFs to date has been conducted on Fe^{III}-MOFs containing trimeric $[Fe_3(\mu_3\text{-}O)(R\text{-}COO)_6(H_2O)_2(OH)]$ SBUs (Fig. 8), which have been demonstrated to tolerate substitution with metals having diverse oxidation states and *r*. These MOFs have been explored for a range of applications in gas adsorption, catalysis and wastewater treatment.[64–75]

Acetate-based molecular trimers of M^{III}, with the formula $[M^{III}_3(\mu_3\text{-}O)(CH_3COO)_6(H_2O)_2(OH)]$, where M^{III} can be V^{III}, Cr^{III}, Mn^{III}, Fe^{III}, Ru^{III}, Rh^{III}, or Os^{III}, have been known since the 1920s and have been extensively investigated for their magnetic properties.[76] These trimers are known to tolerate the reduction of one M^{III} to M^{II}, with the protonation of the OH group to afford compounds with three water molecules as capping ligands and the formula $[M^{III}_2M^{II}(\mu_3\text{-}O)(CH_3COO)_6(H_2O)_3]$.[77–80] Heterobimetallic trimers with the formula $[Fe_2M^{II}(\mu_3\text{-}O)(CH_3COO)_6(H_2O)_3]$, where M^{II} can be Mg^{II}, Mn^{II}, Co^{II}, Ni^{II} or Zn^{II}, were first reported in 1928, and their nature of solid solutions was demonstrated in 1981.[81–83]

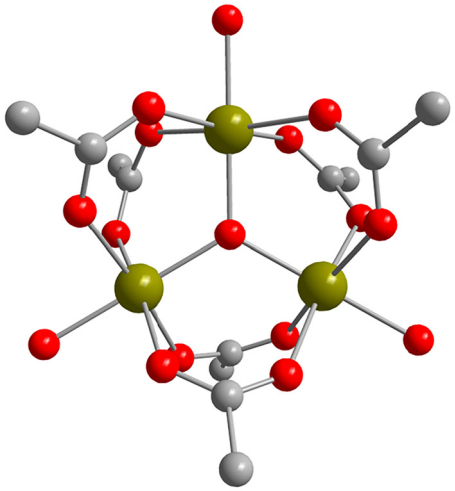

Fig. 8 Structure of the $[Fe_3(\mu_3\text{-}O)(H_2O)_2(OH)(R\text{-}COO)_6]$ SBU. Colour code: Fe, dark yellow; C, grey; and O, red.

In 2014, 34 MOFs based on $[Fe_2M^{II}(\mu_3\text{-}O)(R\text{-}COO)_6(H_2O)_3]$ SBUs, where M^{II} can be Mn^{II}, Co^{II}, Ni^{II} or Zn^{II}, were obtained using a direct synthetic approach starting from heterometallic acetate-based clusters and a range of organic linkers. The coexistence of Fe^{III} and M^{II} was confirmed *via* ICP mass spectrometry (ICP-MS), which revealed that the 2 : 1 Fe^{III}/M^{II} ratio in the molecular precursor was maintained in the final MOF. Among the prepared MOFs, PCN-250 [also known as **soc**-MOF (**soc** is the topology symbol),[84] MIL-127[85] or CPM-200,[86] based on 3,3′,5,5′-azobenzenetetracarboxylate as the organic linker] was found to have exceptional methane storage capacity. The Fe^{III}/Co^{II} analogue was later discovered to display improved CO_2 adsorption capacity and CO_2/N_2 selectivity compared with the homometallic MOF, even under humid conditions.[67]

Later on, a similar synthetic approach was employed to introduce Mg^{II}, Co^{II} and Ni^{II} in the trimeric SBUs of MIL-127, MIL-100 (based on BTC^{3-} as the organic linker) and MIL-88B (based on BDC^{2-} as the organic linker).[65] The MIL-127 analogues and the respective molecular precursors were characterised *via* ^{57}Fe Mössbauer spectroscopy, which proved that the heterometallic nature of trimeric clusters was preserved in the MOF. *In situ* IR spectroscopy using NO as a probe was performed on the heterometallic MIL-127(Fe, Ni) on samples activated under vacuum at 423 K for 3 h and at 503 K for 6 h (Fig. 9a). At 150 K, the spectra of both samples displayed three bands centered at 1895 cm^{-1}, attributed to the Fe^{III}–CO interaction; 1874 cm^{-1}, not present in the homometallic MIL-127 (Fe) and attributed to the Ni^{II}–CO interaction; and 1797 cm^{-1}, attributed to the Fe^{II}–CO interaction and whose intensity is much lower than that of the homometallic analogue,

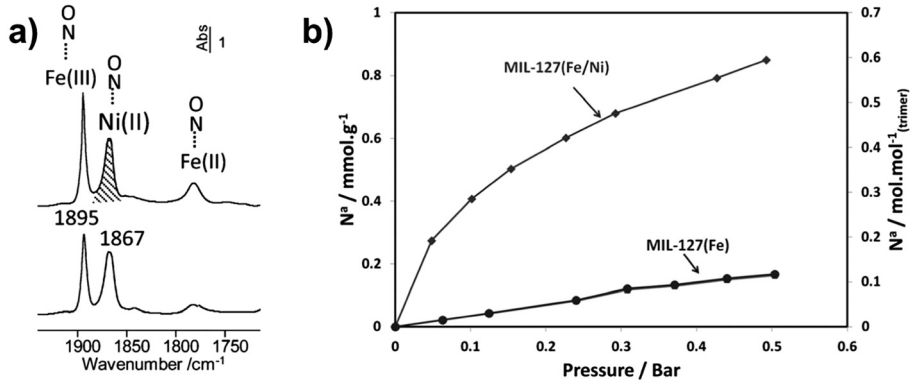

Fig. 9 IR spectra of MIL-127(Fe, Ni) recorded after the introduction of an equilibrium pressure of NO (665 Pa) at 150 K on samples activated under vacuum for 3 hours at 423 K (bottom) and 6 hours at 503 K (top) (a). CO adsorption isotherms of MIL-127(Fe, Ni) and MIL-127(Fe) at 303 K (b). Adapted with permission from ref. 65. Copyright 2015, the Royal Society of Chemistry.

suggesting lower reducibility of Fe^{III} in the presence on Ni^{II}. CO adsorption isotherms collected on MIL-127(Fe) and MIL-127(Fe, Ni) revealed that the latter displays a much higher uptake and heat of adsorption than the homometallic analogue (Fig. 9b), which can be explained by the backdonation effect between Ni^{II} OMSs and CO.

SCXRD analysis revealed that the presence of an additional water molecule in heterometallic $Fe_2^{III}M^{II}$ SBUs in PCN-250 allows to generate up to three Lewis acidic OMSs per SBU upon activation of the aliovalently substituted MOF, as opposed to two sites per SBU in the parent MOF, while decreasing the temperature needed for water desorption (Fig. 10).[74] Further insight into the nature of the OMSs was gained using XANES and *in situ* IR. The XANES spectra of PCN-250(Fe) and PCN-250(Fe_2Ni) collected at the Fe K-edge at increasing temperatures under He flow revealed that the former undergoes significant changes above 484 K, attributed to the reduction of part of Fe^{III} to Fe^{II}, whereas the heterometallic analogue does not undergo a similar process. The presence of OMSs in both MOFs was investigated *via in situ* IR using CO as a probe, finding that PCN-250(Fe) only displays one relatively weak band at 2163 cm^{-1}, associated with the Fe^{III}–CO interaction (the sample was activated at 473 K; therefore, no Fe^{II} was generated), whereas the spectrum of PCN-250 (Fe_2Ni) features a strong band at 2179 cm^{-1}, attributed to the Ni^{II}–CO interaction, accompanied by a weak band at 2163 cm^{-1}, indicative of the concomitant presence of Fe^{III} OMSs.

A water-based synthesis of heterometallic MIL-100 starting from $Fe(SO_4)_2$ and several M^{II} (Mn^{II}, Co^{II}, Ni^{II}, Cu^{II}, Zn^{II}, Cd^{II}) and M^{III} (Al^{III}, Ti^{III}, V^{III}, Cr^{III}, Y^{III}, La^{III}, Ce^{III}, Pr^{III}, Sm^{III}, Tb^{III}) salts (chlorides, nitrates, acetates) was developed in 2020, which led to the oxidation of Fe^{II} to Fe^{III} and the formation of solid solutions with each of the above species, incorporating between 7.5 and 29.9 mol% depending on the cation.[70] XPS revealed that Cu^{II} was reduced to Cu^{I}; Ti^{III} and V^{III} were oxidised to Ti^{IV} and V^{IV}/V^{V}, respectively; and part of Ce^{III} was oxidised to Ce^{IV}. The incorporation of M^{IV} was presumed to be

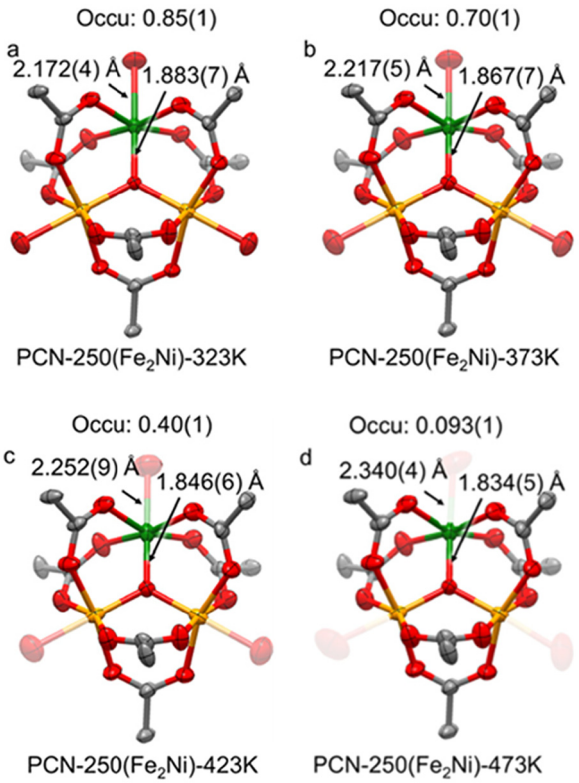

Fig. 10 Single-crystal structures of PCN-250(Fe_2Ni), showing the [Fe_2Ni(μ_3-O)(R-$COO)_6$] cluster and occupancy of terminal O atoms at 323 K (a), 373 K (b), 423 K (c), and 473 K (d). Colour code: Fe, yellow; Ni, green; C, grey; and O, red. Adapted with permission from ref. 74. Copyright 2023, the American Chemical Society.

accompanied by the deprotonation of the OH group to yield an SBU with the formula [Fe_2M^{IV}(μ_3-O)(R-$COO)_6(H_2O)_2$O] with one O^{2-} capping ligand, even though, without further evidence, it cannot be excluded that SBUs with the formula [Fe_2M^{IV}(μ_3-O)(R-$COO)_6(H_2O)(OH)_2$] may also exist (*vide infra*).[87,88] In the case of Cu^{I} substitution, the trimer cannot compensate the excess

negative charge with further protonation of the capping ligands. Therefore, the authors argued that defects might exist, *i.e.*, protonation of part of the carboxylates associated with a reduction of the CN of Cu^{I} to 5, although the IR spectrum does not appear to display bands that can be attributed to −COOH groups. An alternative way of compensating would be to protonate the μ_3-O ligand, as suggested for similar systems discussed herein.[86,89] Defects were also invoked to compensate the excess positive charge generated by the inclusion of V^{V} without further investigation; however, $[Fe_2V^{V}(\mu_3\text{-}O)(R\text{-}COO)_6(OH)_3]$ SBUs might, in principle, exist.

It is interesting to note that attempts to introduce Ni^{II} in MIL-100(Fe) *via* post-synthetic ion metathesis were unsuccessful, which was attributed to the strength of the Fe^{III}–carboxylate bonds preventing the incorporation of softer Ni^{II}.[68] This is in stark contrast to M^{II}-MOFs, where the post-synthetic route appears to be the most effective in achieving aliovalent substitution, perhaps because of the relatively labile M^{II}-carboxylate bonds.

Single crystals of a series of aliovalent solid solutions with 1 : 2 M^{III}/M^{II} ratio (where M^{III} = Sc^{III}, V^{III}, Fe^{III}, Ga^{III}, and In^{III}; M^{II} = Mg^{II}, Mn^{II}, Co^{II}, and Ni^{II}) and **soc** topology were obtained, for which the general formula $[M^{II}_2M^{III}(\mu_3\text{-}OH)(CH_3COO)_6(H_2O)_3]$ was proposed, where charge neutrality is achieved through protonation of the μ_3-O ligand.[86] However, an accurate determination of the chemical composition was not performed. Therefore, it cannot be excluded that extraframework cations exist, *e.g.*, dimethylammonium ($Me_2NH_2^+$) derived from DMA decomposition, used as a solvent for the synthesis, or part of the carboxylate groups be protonated, as proposed for MIL-100 doped with Cu^{I}.[70] SCXRD did not provide direct evidence of the presence of μ_3-OH groups, and the electron density in the pores was treated with the SQUEEZE routine in the PLATON software package, which may result in overlooking the presence of organic cations.[90]

The effect of the aliovalent substitution of Mn^{II} for In^{III} on the proton conduction properties of MOFs with **soc** topology was recently evaluated (Fig. 11).[89] The In^{III}-based MOF differs from the Fe^{III} analogue in that the SBU is positively charged due to the presence of three capping H_2O molecules: $[In_3(\mu_3\text{-}O)(R\text{-}COO)_6(H_2O)_3]^+$. The charged framework is counterbalanced by NO^{3-} anions residing in the pores.[84] For the heterometallic In^{III}/Mn^{II} solid solution with a 1 : 2 ratio, neutral SBUs with the formula $[InMn_2(\mu_3\text{-}OH)(R\text{-}COO)_6(H_2O)_3]$ were proposed, based on previous literature.[86] The homometallic Mn^{II}-based analogue was instead proposed to feature negatively charged SBUs with the formula $[Mn_3(\mu_3\text{-}OH)(R\text{-}COO)_6(H_3O)_{0.5}(H_2O)_{2.5}]^{0.5-}$, with one $Mn(H_2O)_6^{2+}$ cation every four SBUs residing in the pores and warranting charge neutrality. The +2 oxidation state for Mn in all MOFs was confirmed *via* XPS analysis. The proton conductivity moderately increased with progressive substitution of Mn^{II} for In^{III}, with the highest value of 1.15×10^{-2} S cm^{-1} at 328 K and 95% relative humidity (RH) for the homometallic Mn^{II} compound.

The complete aliovalent substitution of Co^{II} and Ti^{IV} for M^{III} was demonstrated in 2013, when MOFs with a MIL-88 topology (dubbed CTOF-1 and CTOF-2, featuring 2-hydroxyterephthalate and BDC^{2-}, respectively, as the organic linker) based on heterometallic SBUs with the formula $[Co_2Ti(\mu_3\text{-}O)(R\text{-}COO)_6O(DMF)_3]$ were reported.[91] The stoichiometry was deduced from the SCXRD data, with ICP atomic emission spectroscopy (ICP-AES) providing supporting information on the chemical composition of the MOF. However, it should be noted that such an SBU would require that one metal atom be 7-coordinated, and it is likely that the actual SBU contains one less DMF molecule, *i.e.*, $[Co_2Ti(\mu_3\text{-}O)(R\text{-}COO)_6O(DMF)_2]$. Different from MIL-88, CTOF-1 and CTOF-2 display permanent porosity when activated, attributed to the existence of two distinct thermodynamically stable phases, as opposed to the continuously swelling MIL-88 framework that collapses to a nonporous phase upon activation.

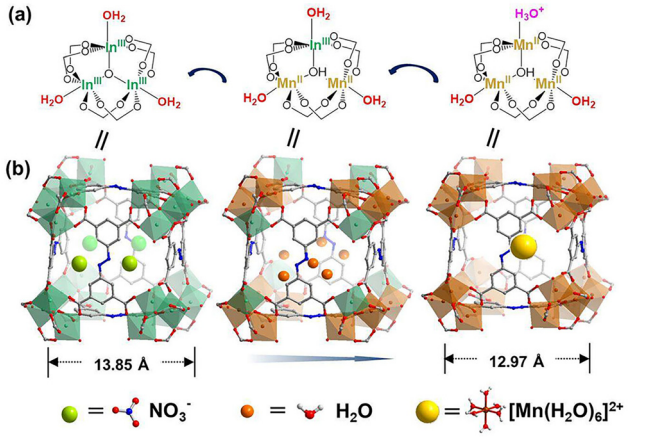

Fig. 11 Trinuclear $M_3(\mu_3\text{-}O)$ clusters (a) and different guest molecules/ions (b) encapsulated in the cubic cages of In-ABTC-H_2O (left), In/Mn-ABTC-H_2O (centre), and $Mn(H_2O)_6$@Mn-ABTC-H_2O (right). Colour code: In, teal; Mn, orange; C, grey; O, red; and N, blue. Reproduced with permission from ref. 89. Copyright 2023, the American Chemical Society.

Soon afterwards, the complete aliovalent substitution of Ti^{IV} for M^{III} was achieved in COK-69 with the formula $Ti_3(\mu_3\text{-}O)(cdc)_3O_2(DMF)$ (where cdc^{2-} is 1,4-cyclohexanedicarboxylate) and MIL-88 topology.[87] The authors performed *ab initio* calculations to determine whether a hydrated SBU would take the form of either $[Ti_3(\mu_3\text{-}O)(R\text{-}COO)_6O_2(H_2O)]$ or $[Ti_3(\mu_3\text{-}O)(R\text{-}COO)_6O(OH)_2]$ and found that they are very close in energy (0.2–0.4 eV per cluster, depending on the functional used). Regardless of the protonation state of the terminal oxo ligands, MOF activation leads to the loss of one water molecule per trimer, affording $[Ti_3(\mu_3\text{-}O)(R\text{-}COO)_6O_2]$ SBUs, featuring one OMS. The energetic cost of removing one water molecule was found to be 6.1 eV per cluster.

The synthesis of homometallic MIL-100(Ti) was achieved by the reaction of $[Ti_6O_6(4\text{-}tbbz)_6(O^iPr)_6]$ (where $tbbz^-$ is 4-*tert*-butylbenzoate) clusters with H_3BTC in acetonitrile/tetrahydrofuran. This allowed to draw comparisons with the M^{III}-based archetype, demonstrating that MIL-100(Ti) is more thermally and chemically stable, thanks to the stronger Ti^{IV}–O bonds.[88] Independent calculations confirmed that the two forms of the

hydrated SBU, *i.e.*, $[Ti_3(\mu_3\text{-}O)(R\text{-}COO)_6O_2(H_2O)]$ and $[Ti_3(\mu_3\text{-}O)(R\text{-}COO)_6O(OH)_2]$, are very close in energy. The CO_2 and H_2O adsorption properties are comparable between the two MOFs, suggesting that the chemistry of the SBU plays a relatively minor role when the structure features very large pores and adsorbate/adsorbate interactions prevail.

Heterometallic Ti^{IV}/M^{II} MIL-100 analogues were successively prepared by reacting Ti^{IV}-isopropoxide with the chloride salts of Mg^{II}, Fe^{II}, Co^{II} and Ni^{II}.[92] In the case of Fe, Mössbauer spectroscopy revealed that it was oxidized to Fe^{III}, affording a solid solution between MIL-100(Fe) and MIL-100(Ti), named MUV-101(Fe), with a Fe^{III}/Ti^{IV} ratio of 2 : 1 and proposed formula $Fe_2Ti(\mu_3\text{-}O)(BTC)_2(H_2O)(OH)_2$. The solid solution nature of MUV-101(Fe) was ascertained *via* pair distribution function analysis, which revealed the presence of two sets of M–M distances within the trimer, associated with the Ti^{IV}–Fe^{III} and Fe^{III}–Fe^{III} pairs, respectively (Fig. 12). Water adsorption isotherms suggest the formation of 1.68 OMSs per trimer upon activation, as opposed to 2.70 for MIL-100(Fe), compatible with the additional positive charge on Ti^{IV} in MUV-101(Fe). MUV-101(Fe) shows higher stability than the analogues containing Mg^{II}, Co^{II} and Ni^{II} and was tested as a catalyst for the detoxification of chemical warfare simulants in non-buffered conditions and compared with homometallic MIL-100(Fe) and MIL-100(Ti). The aliovalent MUV-101(Fe) demonstrated a much higher catalytic activity, which was attributed to the synergetic cooperation of Ti^{IV} Lewis acid and Fe(III)–OH Brønsted acid sites. The presence of such sites was ascertained *via in situ* FT-IR spectroscopy using CO as a probe, which revealed that MUV-101(Fe) is unique among heterometallic analogues in that it features a band at 2154 cm^{-1}, attributed to the interaction of CO with OH groups coordinated to Fe^{III}.[93] The thermal decomposition of MUV-101(Fe) results in the formation of carbon-supported titanomaghemite nanoparticles with a Fe/Ti ratio close to 2, not achievable by soft-chemistry routes, that demonstrate outstanding catalytic activity for the production of CO from CO_2 *via* the reverse water–gas shift reaction.[94]

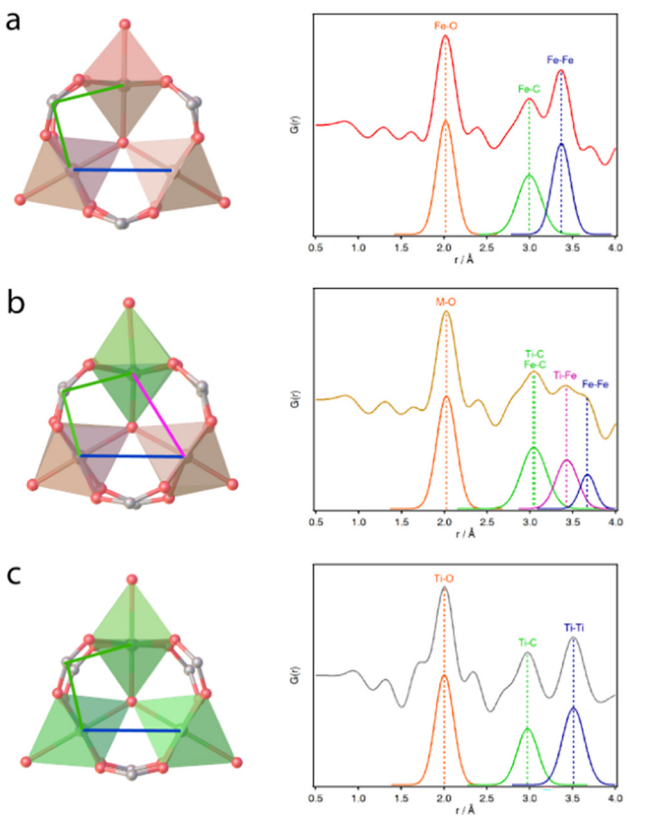

Fig. 12 Structures of SBUs (left) and deconvolution of the experimental differential PDFs (right) for MIL-100(Fe) (a), MUV-101(Fe) (b), and MIL-100(Ti) (c). Colour code: Fe, orange; Ti, green; C, grey; and O, red. Reproduced with permission from ref. 92. Copyright 2023, the American Chemical Society.

Heterometallic MUV-101 was also shown to be accessible starting from MUV-10 through post-synthetic exchange of Ca^{II} with Fe^{II}, Co^{II}, Ni^{II}, and Zn^{II}. The formation of trimeric SBUs with TiM^{II}_2 stoichiometry, with all metals in octahedral geometry (CN 6), is thermodynamically more favourable than the tetrameric $Ti_2M^{II}_2$ found in pristine MUV-10, where M^{II} is in capped trigonal antiprismatic geometry (CN = 7), for Fe, Ni and Co, with energies ranging between −13.6 and −10.0 eV, whereas in the case of Zn^{II}, the difference is only 0.9 eV. It was demonstrated that all the above metals could be incorporated in MUV-101 starting from MUV-10. The process of conversion from the starting MUV-10 to the final MUV-101 phase was investigated *via* scanning electron microscopy (SEM), which suggested that the formation of the MUV-101 phase proceeds *via* crystal-to-crystal transformation, rather than by dissolution of MUV-10 in the reaction medium and recrystallisation of MUV-101.[95] An analogous post-synthetic approach was also employed to obtain heterometallic MUV-301(Ti/Co), an isoreticularly expanded version of MUV-101 based on the organic linker benzo-tris-thiophene carboxylate, starting from MUV-30, which displays the same topology of MUV-10.[96]

Another prominent family of M^{III}-MOFs is represented by MIL-53 and related frameworks based on monodimensional inorganic units consisting of 6-coordinated M^{III} connected through carboxylates and the μ_2-OH groups (Fig. 13). The aliovalent substitution of V^{IV} for Al^{III} in MIL-53, with the formula $Al(\mu_2\text{-}OH)(BDC)$, and the analogue based on 1,4-naphthalenedicarboxylate was initially reported in 2013, leveraging on the isoreticular relationship between MIL-53 and the V^{IV}-based MIL-47, with the formula $V(\mu_2\text{-}O)(BDC)$.[97] A series of samples for each system was prepared *via* direct synthesis varying the Al/V molar ratios in a stepwise fashion. The solid solution nature of the heterometallic compounds was suggested by PXRD, which revealed a single crystalline phase with lattice parameters linearly varying in agreement with Vegard's law. Further insight was provided by ^1H and ^{13}C solid-state nuclear magnetic resonance (SSNMR) as well as EPR and IR spectroscopies, which collectively pointed to the general formula $(AlOH)_{1-x}(VO)_x(BDC)$, indicating the deprotonation of bridging OH groups to compensate the excess positive charge generated by the substitution of V^{IV} for Al^{III}. The effect of V^{IV} incorpor-

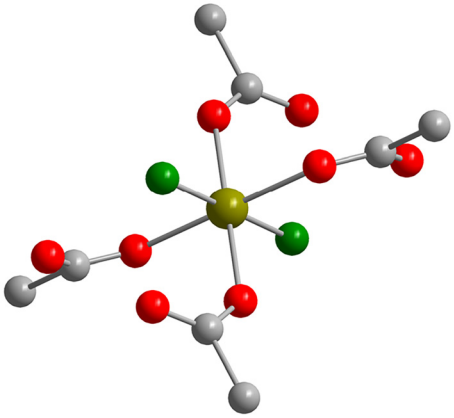

Fig. 13 Coordination environment of M^{III} in MIL-53. Colour code: M^{III}, dark yellow; C, grey; O, red; and μ_2-OH, green.

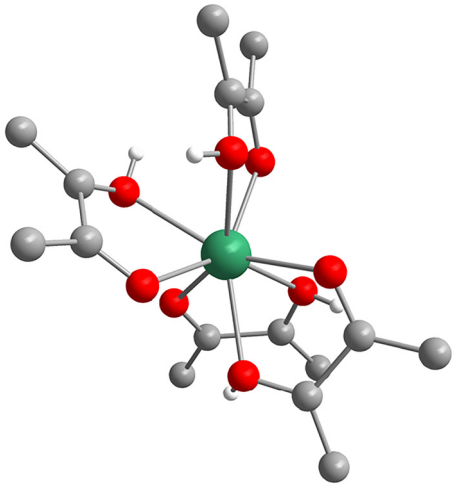

Fig. 14 Coordination environment of In^{III} in In-BQ. Colour code: In, sea green; C, grey; O, red; and H, white.

ation on the breathing behaviour of MIL-53 upon CO_2 adsorption was evaluated, finding that increasing amounts of V^{IV} progressively inhibited framework flexibility, which is to be expected given the rigid character of MIL-47. The same concept was applied to DUT-5, with the formula Al(μ_2-OH)(BPDC) (where $BPDC^{2-}$ is 4,4′-biphenyldicarboxylate), and COMOC-2, with the formula V(μ_2-O)(BPDC), with the difference that Al-based DUT-5 is rigid, whereas V-based COMOC-2 is flexible, and the aliovalent solid solutions display an intermediate behaviour.[98] Other works have investigated similar aliovalent solutions with the aim of identifying the location of V^{IV} sites and to gather further insight into their breathing behaviour.[99–102]

The aliovalent substitution of Ni^{II} was demonstrated in InOF-1, with the formula $In_2(\mu_2\text{-}OH)_2(BPTC)$ (also known as NOTT-300 or MFM-300,[103] where $BPTC^{4-}$ is 3,3′,5,5′-biphenyl tetracarboxylate), which features similar extended inorganic units to those found in MIL-53, with 6-coordinated In^{III}.[104] Aliovalent substitution, accomplished *via* direct synthesis in the presence of formic acid, led to the formation of NiOF-1, with the formula $Ni_2(BPTC)(HCOOH)_2$, where charge compensation is warranted by neutral formic acid, coordinated in a bridging fashion through the carbonyl oxygen, replacing anionic OH groups in the inorganic unit. The presence of acidic protons from formic acid and the larger amount of adsorbed water molecules in the channels led to a five-fold increase in proton conduction in NiOF-1 compared with InOF-1 (3.41×10^{-2} S cm^{-1} *vs.* 7.86×10^{-3} S cm^{-1}, respectively, at 328 K and 95% RH).

The MOF In-BQ, with the formula $(Me_2NH_2)(Me_2NH)[In(mdhbqdc)_2]$ (where $mdhbqdc^{2-}$ is dimethyl 3,6-dihydroxy-2,5-benzoquinone-1,4-dicarboxylate), features isolated 8-coordinated In^{III} and one extraframework $Me_2NH_2^+$ cation per In^{III}, counterbalancing the negatively charged framework (Fig. 14).[105,106] The replacement of In^{III} with Cd^{II} affords isostructural Cd-BQ, with the formula $(Me_2NH_2)_2[Cd(mdhbqdc)_2]$, where two extraframework $Me_2NH_2^+$ cations per Cd^{II} exist, as a means to compensate for the excess negative charge produced by aliovalent substitution. The proton conductivity of Cd-BQ was found to be two orders of magnitude higher than that of In-BQ (2.30×10^{-2} S cm^{-1} *vs.* 2.10×10^{-4} S cm^{-1}, respectively, at 303 K and 95% RH), thanks to the higher density of $Me_2NH_2^+$ in the pores, which are engaged in an extended network of hydrogen bonds warranting high mobility to the charge carriers.

An unusual charge compensation mechanism involving oxidation of the organic linker was recently reported in the 2D MOF $Fe_3(THT)_2$ (where THT is triphenylenehexathiol) when Fe^{III} was aliovalently substituted by Ni^{II}.[107] $Fe_3(THT)_2$ is based on isolated square-planar (CN 4) Fe^{III} centres (Fig. 15) and exhibits high electronic conductivity and charge mobility. Complete exchange of Ni^{II} for Fe^{III} was accomplished post-synthesis, and the preservation of the +2 oxidation state for Ni was confirmed *via* XPS analysis. The possible presence of extraframework $Me_2NH_2^+$ cations was excluded based on CHN elemental analysis as well as IR and NMR spectroscopies.

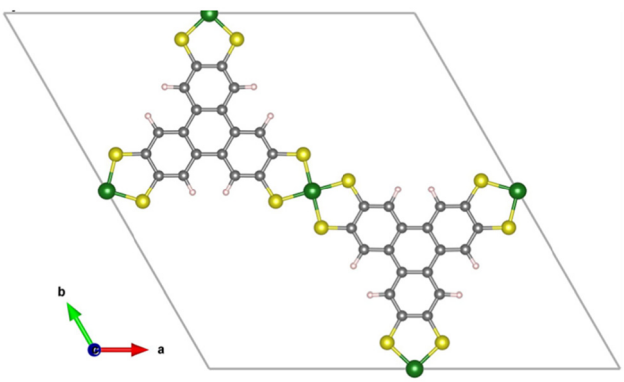

Fig. 15 Crystal structure of $Fe_3(THT)_2$ viewed along the *c* axis. Colour code: Fe, green; C, grey; S, yellow; and H, white. Reproduced with permission from ref. 107. Copyright 2023, the American Chemical Society.

High-resolution S 2p XPS analysis revealed instead multiple overlapping signals between 162 and 166 eV, displaying an overall shift toward higher energy than $Fe_3(THT)_2$ and suggesting that the linker is oxidised after replacement of Fe^{III} with Ni^{II}. The bulk electrical conductivity of $Ni_3(THT)_2$ was found to be four times higher than $Fe_3(THT)_2$ (0.32 S cm^{-1} *vs.* 0.078 S cm^{-1}, respectively). The measured Hall carrier concentration at room temperature in $Ni_3(THT)_2$ decreases 60-fold to 6.43×10^{18} cm^{-3} from $Fe_3(THT)_2$ ($3.97(7) \times 10^{20}$ cm^{-3}), whereas the calculated Hall mobility increases 50-fold to 0.37 cm^2 V^{-1} s^{-1} compared with the value in $Fe_3(THT)_2$ (0.017 cm^2 V^{-1} s^{-1}). The increased Hall mobility in $Ni_3(THT)_2$ was ascribed to the higher covalency of S–Ni^{II} bonds.

M^{IV}-MOFs

M^{IV}-MOFs (M^{IV} = Ti^{IV}, Zr^{IV}, Ce^{IV}, Hf^{IV}, Th^{IV}, U^{IV}, and Pu^{IV}) commonly feature CNs of 6 (Ti^{IV}) and 8 (Zr^{IV}, Ce^{IV}, Hf^{IV}, Th^{IV}, U^{IV}, and Pu^{IV}) and have been shown to undergo aliovalent substitution with M^{II} and M^{III}. The inclusion of subvalent M^{II}/M^{III} yields a framework with an excess negative charge, which is usually compensated by the protonation of O/OH groups in the inorganic unit, although anion vacancies have also been proposed. In principle, supervalent M^{V} could also substitute for M^{IV}, generating an excess positive charge that could be compensated by the deprotonation of OH groups in the inorganic unit.

M^{IV}-MOFs based on hexanuclear SBUs with the formula $[M^{IV}_6(\mu_3\text{-O})_4(\mu_3\text{-OH})_4(\text{R-COO})_{12}]$, where each M^{IV} (Zr^{IV}, Ce^{IV}, Hf^{IV}, Th^{IV}, U^{IV}, Pu^{IV}) is 8-coordinated by two μ_3-O, two μ_3-OH and four carboxylic oxygens (Fig. 16a), are a prominent family of MOFs first reported in 2008.[108–114] Inorganic units derived from the condensation of hexanuclear M^{IV} oxo/hydroxo clusters were also discovered, further expanding the accessible topological space: dodecanuclear clusters with the formula $[M^{IV}_{12}O_8(OH)_{14}(\text{R-COO})_{18}]$ and one-dimensional inorganic building units with the general formula $[M^{IV}_5O_4(OH)_4(\text{R-COO})_8]_n$.[115,116] Interestingly, the $[M^{IV}_6(\mu_3\text{-O})_4(\mu_3\text{-OH})_4]^{12+}$ clusters have the same local M^{IV}–O connectivity found in the fluorite-like cubic polymorphs of ZrO_2 and HfO_2 and in CeO_2 (Fig. 16b). Thus, these MOFs are an ideal bridge between inorganic solid-state chemistry and reticular chemistry.

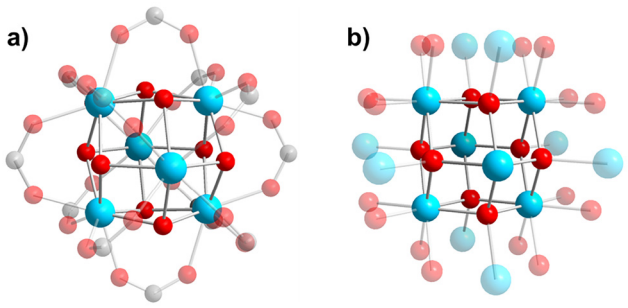

Fig. 16 Local M^{IV}–O connectivity in the $[M^{IV}_6(\mu_3\text{-O})_4(\mu_3\text{-OH})_4(\text{R-COO})_{12}]$ SBUs (a) and in fluorite-type M^{IV} oxides (b). Atoms not belonging to the $[(M^{IV})_6O_4(OH)_4]$ clusters are shaded to highlight the similarity between the two local structures. Colour code: M^{IV}, cyan; C, grey; and O, red.

As mentioned in the introduction, the aliovalent substitution of M^{III} or M^{II} in fluorite-type $M^{IV}O_2$ generates oxygen vacancies, yielding non-stoichiometric oxides with the general formula $M^{IV}_{1-x}M^{III}_xO_{2-0.5x}$ or $M^{IV}_{1-x}M^{II}_xO_{2-x}$. The amount of aliovalent metal that can be introduced before segregation of two distinct crystalline phases occurs is limited by the excessive strain induced by a large number of oxygen vacancies in the fluorite-type structure. In the case of industrially relevant yttria-stabilised zirconia, complete solid solubility occurs in a rather wide range of compositions comprised between ~16 and ~67% Y^{III} mol%.[117]

Notably, the same type of metal oxo/hydroxo clusters found in M^{IV}-MOFs have been obtained using Ln^{III} (r = 0.99–1.16 Å, CN 8).[118,119] The excess negative charge in the Ln^{III}-based clusters is thought to be compensated through either protonation of the μ_3-O bridges or their substitution with fluoride to render the formula $[Ln^{III}_6(\mu_3\text{-OH/F})_8(\text{R-COO})_{12}]^{2-}$, plus the inclusion of two extraframework cationic species per SBU (most often $Me_2NH_2^+$ derived from the decomposition of DMF during the synthesis) to provide the necessary positive charges to preserve electroneutrality. The incorporation of fluoride ions, abstracted from the fluorinated coordination modulators typically used during the synthesis, appears to be crucial to enable the formation of hexanuclear clusters instead of other inorganic units with different nuclearity levels.[120,121] The existence of $[Ln^{III}_6(\mu_3\text{-OH/F})_8(\text{R-COO})_{12}]^{2-}$ SBUs suggests that a continuous solid solution could, in principle, be formed between the end members when M^{IV} and Ln^{III} (and possibly other M^{III} species) with similar r are combined, potentially enabling fine-tuning of the composition and physico-chemical properties. However, it should be noted that in the case of isovalent Zr^{IV}/Ce^{IV} solid solutions, it was demonstrated that only three types of clusters exist: Zr_6, Zr_5Ce, and Ce_6.[39,40] This is likely due to the relatively large difference in r between Zr^{IV} and Ce^{IV}, which might induce excessive strain in the clusters if more than one Ce^{IV} is incorporated.

There have been recent reports focusing on the introduction of aliovalent metals in Zr^{IV}-MOFs in the literature;[122–130] however, convincing evidence of the effective incorporation of the aliovalent species Mg^{II} and Ce^{III} in the SBUs of Zr^{IV}-MOFs was only provided in three cases.[126,129,130]

The first attempt to incorporate Ce^{III} in UiO-66/67(Zr) dates back to 2013;[122] however, it was only in 2021 that the presence of Ce^{III} within the clusters of UiO-66 was demonstrated.[129] ICP analysis revealed that 4 wt% of Ce was incorporated in the MOF (about 0.5 Ce per SBU), both when the synthesis was performed without modulator and when formic acid was used, despite the 1 : 1 Zr/Ce ratio in the reaction mixture. The authors noted how limited information on the presence of Ce^{III} in the clusters could be gathered *via* XPS, whereas compelling evidence was provided by EXAFS at the Zr K-edge and XANES at the Ce L_3-edge (Fig. 17). EXAFS at the Zr K-edge suggests that Ce is effectively incorporated in the SBUs, causing a progressive decrease of the intensity of the feature at

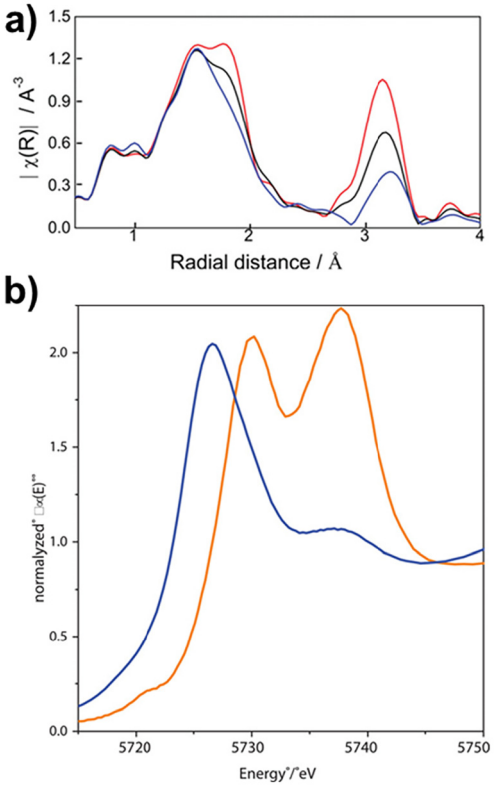

Fig. 17 Fourier transform of the EXAFS signal of the spectra of UiO-66 (Zr) (red), UiO-66(Zr,Ce) prepared with formic acid (blue) and UiO-66(Zr, Ce) prepared without formic acid (black), at the Zr K-edge (a). XANES region of the Ce L_3-edge spectrum of UiO-66(Zr,Ce) prepared with formic acid (blue), UiO-66(Zr,Ce) prepared without formic acid (black), CeO_2 (dotted green line), and $Ce(NO_3)_3{\cdot}6H_2O$ (dotted orange line) (b). Adapted with permission from ref. 129. Copyright 2021, Wiley–VCH GmbH.

3.15 Å in the Fourier transform of the EXAFS signal, associated with Zr–Zr distances. XANES at the Ce L_3-edge confirms that the use of formic acid is crucial to prevent oxidation of 50% of Ce^{III} to Ce^{IV} when starting from $Ce(NO_3)_3$ as a precursor. The authors also demonstrated that the addition of Pt nanoparticles during the synthesis favours the decomposition of formic acid and the subsequent reduction of Ce^{IV} when starting from $(NH_4)_2Ce(NO_3)_6$. In terms of charge compensation mechanism, it was proposed that each Ce^{III} atom induces vacancies of two carboxylate ligands (one BDC linker), based on the decrease in the Zr–O contribution at 1.81 Å in the Fourier transform of the EXAFS signal as the Ce^{III} content increases. The authors suggested that an OH ligand should take the place of a missing carboxylate oxygen to warrant charge neutrality and keep the eightfold coordination of the Zr^{IV} atoms, which would afford an SBU with the formula $[Zr_5Ce(\mu_3\text{-}O)_4(\mu_3\text{-}OH)_4(R\text{-}COO)_{10}(OH)]$, where the available oxygens fill 45 coordination positions, suggesting that three additional neutral ligands, most likely water molecules, are needed to warrant a CN of 8 for all metals in the SBU.

$[Mg(OMe)_2(MeOH)_2]_4$ was used as a source of Mg^{II} to perform post-synthetic exchange on three Zr^{IV}-MOFs: UiO-66 with the formula $Zr_6O_4OH_4(BDC)_6$, MOF-808 with the formula $Zr_6O_4OH_4(HCOO)_6(BTC)_2$, and NU-1000 with the formula $Zr_6O_4OH_4(HCOO)_4(TBAPy)_2$ [where $TBAPy^{4-}$ is 1,3,6,8-tetrakis (*p*-benzoate)pyrene].[126] No exchange was achieved in UiO-66, whose pores are too small to allow diffusion of $[Mg(OMe)_2(MeOH)_2]_4$, whereas MOF-808 and NU-1000 incorporated up to 0.64 Mg^{II} per SBU. Using EXAFS at the Zr K-edge, the incorporation of Mg^{II} in the SBU was ascertained based on the decrease in the intensity of the $\chi(r)$-signal at ~3.1 Å, corresponding to Zr–Zr distances within octahedral Zr-clusters (Fig. 18). The charge compensation mechanism was assumed to involve protonation of two μ_3-O, leading to the formulation of the heterometallic SBUs as $[Zr_5Mg(\mu_3\text{-}O)_2(\mu_3\text{-}OH)_6(R\text{-}COO)_{12}]$, with 8-coordinated Mg^{II}. The aliovalent solid solutions were found to be more active for nerve agent detoxification than the parent MOFs, which was attributed to the synergistic effect of the increased nucleophilicity of OH^-/O^{2-} residues and charge gradients in the $[Zr_5Mg(\mu_3\text{-}O)_2(\mu_3\text{-}OH)_6]^{12+}$ heteronuclear cluster, facilitating the hydrolytic cleavage of polar P–X bonds (X = F, OR, or SR).

A very recent paper investigated a similar Mg^{II}-containing MOF-808(Zr) as a catalyst for the hydrolysis of dipeptides and phosphoesters and provided additional insight into the structure of the SBUs.[130] EXAFS at the Zr K-edge on the MOF activated under vacuum at 393 K for 17 hours suggested that anion vacancies were formed to compensate for the excess negative charge and the clusters contained only 7.3 and 6.8 oxo/hydroxo bridges when either one or two Mg^{II} were incorporated, respectively, as determined *via* ICP analysis. This was attributed to the fact that Mg^{II} preferentially adopts a 6-coordinated geometry, which, in turn, forces Zr to a lower CN than 8, thereby increasing the availability of Lewis acidic sites and favouring the catalytic activity (Fig. 19). The authors did not delve further into the

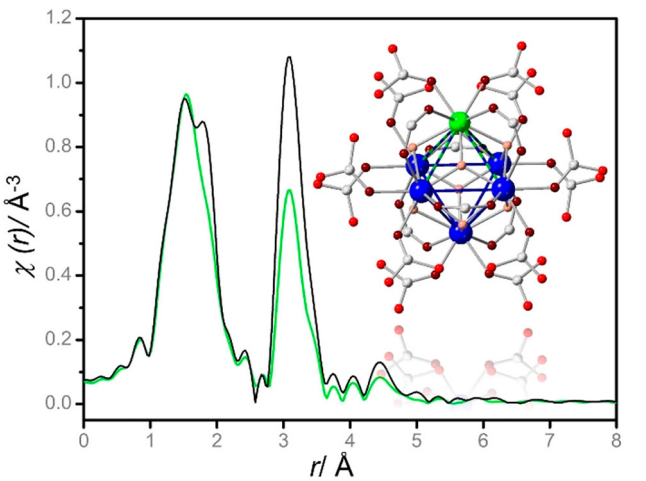

Fig. 18 *k*2-weighted $\chi(r)$ Zr K-edge EXAFS data collected on pristine MOF-808 (black) and Mg^{II}-doped MOF-808 (green). The inset shows the $[Zr_5Mg(\mu_3\text{-}O)_2(\mu_3\text{-}OH)_6(R\text{-}COO)_{12}]$ model in the doped system. Colour code: Mg, green; Zr, blue; C, grey; and O, red. Reproduced with permission from ref. 126. Copyright 2019, the American Chemical Society.

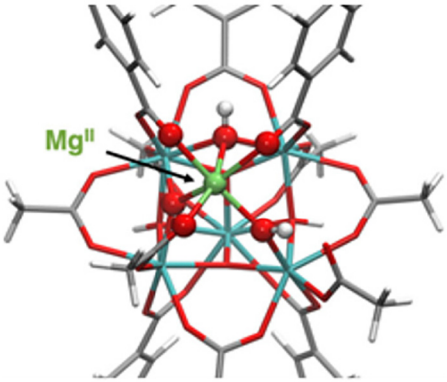

Fig. 19 Optimised structure of a Zr_5Mg node. The Mg^{II} ion and the groups directly bonded to it are represented as spheres, while the rest of the structure is shown as sticks. Colour code: Mg, lime; Zr, cyan; C, grey; O, red; and H, white. Reproduced with permission from ref. 130. Copyright 2025, the American Chemical Society.

charge compensation mechanism; however, the formulas $[Zr_5Mg(\mu_3\text{-}O)_{2.7}(\mu_3\text{-}OH)_{4.6}(R\text{-}COO)_{12}]$ and $[Zr_4Mg_2(\mu_3\text{-}O)_{1.2}(\mu_3\text{-}OH)_{5.6}(R\text{-}COO)_{12}]$ can reasonably be proposed for the SBUs, assuming that the activation procedure employed does not induce dehydroxylation of the clusters, usually achieved at temperatures exceeding 473 K under dynamic vacuum.[131]

Ti^{IV}-MOFs commonly feature 6-coordinated Ti^{IV} centres, which can self-assemble in a variety of SBUs with nuclearities ranging from 1 to 12. Among these, aliovalent substitution has been achieved on trimers with the formula $[Ti_3(\mu_3\text{-}O)(R\text{-}COO)_6O(OH)_2]$, already discussed above as aliovalent analogues of M^{III}-based MOFs, and on octamers with the formula $[Ti_8(\mu_2\text{-}O)_8(\mu_2\text{-}OH)_4(R\text{-}COO)_{12}]$, found in MIL-125, where Ti^{IV} is 6-coordinated in octahedral geometry (Fig. 20).[132]

NH_2-MIL-125, with the formula $Ti_8(\mu_2\text{-}O)_8(\mu_2\text{-}OH)_4(NH_2\text{-}BDC)_6$ (where $NH_2\text{-}BDC^{2-}$ is 2-amino-1,4-benzenedicarboxylate), has been intensely investigated for its photocatalytic properties, thanks to a band gap of 2.6 eV that allows it to absorb visible light *via* linker-to-metal cluster charge transfer.[133,134] Several studies appeared in the literature proposing the modification of NH_2-MIL-125 with $Fe^{II/III}$, Ni^{II}, Co^{II}, and Cu^{II}, as a means to improve the photocatalytic performance; however, no proof was provided regarding the effective incorporation of such species in the SBU.[135–138] The possibility to tune the electronic structure of NH_2-MIL-125 by aliovalent substitution was proposed in a theoretical study[125] and demonstrated experimentally in 2020 by incorporating Fe^{III} using a direct synthesis approach.[139] Atomic absorption spectroscopy was employed to quantify the amount of Fe^{III} incorporated, which was found to be 1.1 atoms per SBU, in agreement with the stoichiometry of the reaction mixture. XANES at the Fe K-edge revealed that the pre-edge feature and edge shift of the spectrum of Fe-substituted NH_2-MIL-125 resembled those of $\alpha\text{-}Fe_2O_3$, where Fe^{III} is in octahedral coordination. Fitting of the EXAFS spectrum was performed using a model derived from the reported crystal structure of NH_2-MIL-125, in which a Ti site was substituted with Fe, demonstrating longer average first shell Fe–O bond lengths compared with those of the Ti sites found in the parent MOF, in agreement with the slightly larger r of Fe^{III}. The authors did not discuss the charge compensation mechanism, which is likely to involve the protonation of μ_2-O ligands, affording SBUs with the formula $[Fe_{1.1}Ti_{6.9}(\mu_2\text{-}O)_{6.9}(\mu_2\text{-}OH)_{5.1}(R\text{-}COO)_{12}]$. The incorporation of Fe^{III} was also attempted by post-synthetic exchange, soaking NH_2-MIL-125 in a $FeCl_3$ solution but was not successful. The photochemical properties of the homometallic and Fe^{III}-doped NH_2-MIL-125 were investigated *via* optical and X-ray transient absorption spectroscopies, observing a longer photogenerated carrier lifetime in the heterometallic MOF, attributed to the Fe dopant acting as a trap site for electrons and serving to delay electron–hole recombination. The same authors later reported on the effect of varying Fe^{III} contents on the photocatalytic performance of NH_2-MIL-125, testing samples with 0.5, 1 and 2 Fe^{III} per SBU for the degradation of rhodamine B upon photoirradiation with 400–700 nm light and finding that a higher Fe content led to faster degradation.[140]

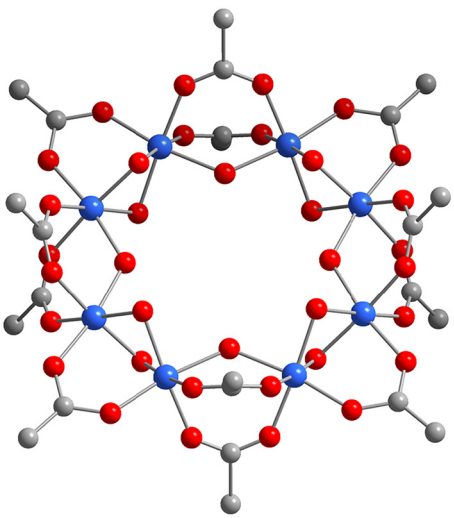

Fig. 20 Structure of the $[Ti_8(\mu_2\text{-}O)_8(\mu_2\text{-}OH)_4(R\text{-}COO)_{12}]$ SBUs. Colour code: Ti, blue; C, grey; and O, red.

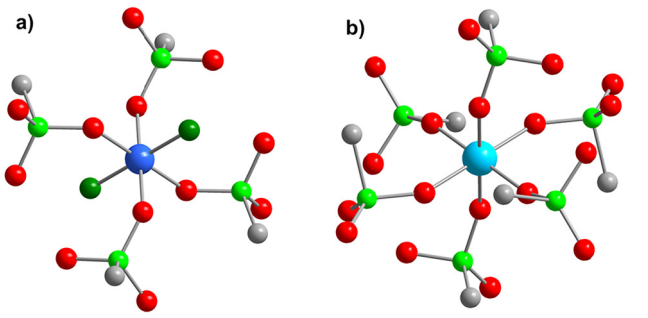

Fig. 21 Coordination environments of Ti^{IV} in MIL-91 (a) and Zr^{IV} in $[Zr_2H_4(PMP)_3]$ (b). Colour code: Ti, blue; Zr, cyan; P, light green; C, grey; O, red; and μ_2-O, green.

Table 3 Examples of the aliovalent solid solutions of MOFs discussed in this perspective

Inorganic unit	Original ion	Aliovalent ion	Charge compensation	Ref.
$[Cd_4(\mu_4\text{-}O)(R\text{-}COO)_8(CH_3OH)_4]^{2-}$	Cd^{II}	Nd^{III}, Dy^{III}	Addition of extraframework NO_3^-	43
$[Mn_4(\mu_4\text{-}Cl)(R\text{-}COO)_8(DMF)_4]^-$	Mn^{II}	Fe^{III}	Addition of μ_2-O ligands	44
$[Zn_4(\mu_4\text{-}O)(R\text{-}COO)_6]$	Zn^{II}	Ti^{III}, V^{III}, Cr^{III}	Addition of Cl^- ligands	29
$[Cu_2(R\text{-}COO)_4(H_2O)_2]$	Cu^{II}	Ti^{IV}	Deprotonation of H_2O ligands	45
$Ni_2(DOBDC)(H_2O)_2$	Ni^{II}	Fe^{III}	Substitution of H_2O ligands with Cl^-	46
$[Zn_5Cl_4(btdd)_3]$	Zn^{II}	Li^{I}, Cu^{I}	Loss of Cl^- ligands	47 and 48
		Cr^{III}	Addition of Cl^- ligands	63
$[M_3(\mu_3\text{-}O)(R\text{-}COO)_6(H_2O)_2(OH)]$	Fe^{III}	Mg^{II}, Mn^{II}, Co^{II}, Ni^{II}, Zn^{II}, Cd^{II}	Protonation of OH ligands	64, 65, 70 and 74
		Ti^{IV}, V^{IV}, Ce^{IV}	Deprotonation of H_2O ligands	70, 87 and 88
$[In_3(\mu_3\text{-}O)(R\text{-}COO)_6(H_2O)_3]^+$	In^{III}	Mn^{II}	Protonation of μ_3-O ligands	89
$Al(\mu_2\text{-}OH)(BDC)$	Al^{III}	V^{IV}	Deprotonation of μ_2-OH ligands	97
$In_2(\mu_2\text{-}OH)_2(BPTC)$	In^{III}	Ni^{II}	Replacement of μ_2-OH ligands with HCOOH	104
$[In(mdhbqdc)_2]^+$	In^{III}	Cd^{II}	Protonation of extraframework Me_2NH	105
$Fe_3(THT)_2$	Fe^{III}	Ni^{II}	Oxidation of the linker	107
$[Zr_6(\mu_3\text{-}O)_4(\mu_3\text{-}OH)_4(R\text{-}COO)_{12}]$	Zr^{IV}	Ce^{III}	Replacement of BDC with OH ligands	129
$[Zr_6(\mu_3\text{-}O)_4(\mu_3\text{-}OH)_4(R\text{-}COO)_{12}]$	Zr^{IV}	Mg^{II}	Protonation of μ_3-O ligands or formation of μ_3-O/μ_3-OH vacancies	126 and 130
$[Ti_8(\mu_2\text{-}O)_8(\mu_2\text{-}OH)_4(R\text{-}COO)_{12}]$	Ti^{IV}	Fe^{III}	Protonation of μ_2-O ligands	139
$[TiO(H_2PMP)]$	Ti^{IV}	Al^{III}	Protonation of terminal O ligands	141
$[Zr_2H_4(PMP)_3]$	Zr^{IV}	Al^{III}	Protonation of non-coordinating P–O groups	142 and 143

Shifting the focus to the more niche area of phosphonate-based MOFs, the aliovalent substitution of Al^{III} for either Ti^{IV} or Zr^{IV} is possible in two MOFs derived from *N*,*N*′-piperazine-bis(methylene-phosphonic acid) (H_4PMP): MIL-91, with the formula $Ti(\mu_2\text{-}O)(H_2PMP)$,[141] and $Zr_2H_4(PMP)_3$,[142,143] both featuring 1D inorganic units and 6-coordinated M^{IV} (Fig. 21). The different linker/metal ratios and coordination environments of Ti^{IV} and Zr^{IV}, though, lead to different charge compensation mechanisms when Al^{III} is introduced. In MIL-91, Ti^{IV} is coordinated by five O atoms belonging to phosphonate groups and one bridging μ_2-O atom, and its replacement with Al^{III} is accompanied by the protonation of the latter, yielding $Al(\mu_2\text{-}OH)(H_2PMP)$. In $Zr_2H_4(PMP)_3$, Zr^{IV} is coordinated by six O atoms belonging to phosphonate groups, and its replacement with Al^{III} is accompanied by the protonation of two non-coordinating P–O groups, yielding $Al_2H_6(PMP)_3$ (CAU-60). Notably, the same framework can be obtained with several M^{III} (Ga, V, Fe, Sc, In, Lu, Yb, Y, and Dy), with *r* ranging between 0.62 and 0.912 Å. The formation of aliovalent solid solutions in either MIL-91 or CAU-60 is not documented, although in principle, both frameworks might be able to tolerate the presence of either Al^{III} or Sc^{III}, respectively, as observed in the NASICON-type ion conductors $Li_{1+x}Al_xTi_{2-x}(PO_4)_3$, $Na_3Sc_xZr_{2-x}(SiO_4)_{2-x}(PO_4)_{1+x}$ and $Na_2Sc_xZr_{2-x}(SiO_4)_{1-x}(PO_4)_{2+x}$.[144,145]

Conclusions

The available literature discussed herein and summarised in Table 3 suggests that aliovalent substitution can be achieved in MOFs *via* either direct synthesis or post-synthetic exchange and that a range of charge-compensation mechanisms is possible. The local structure of the inorganic unit determines the possible charge-compensation mechanisms: systems that contain –O, –OH or H_2O ligands can easily compensate the excess charge *via* addition/removal of protons, whereas systems without such ligands primarily rely on the addition/removal of anions, either within the coordination sphere of the metal or in extraframework positions. The presence of aliovalent metals in the resulting solid solutions leads to the emergence of new properties, particularly when the homometallic isoreticular analogue based on the aliovalent species is not synthetically accessible. Yet, the concept of aliovalent substitution in MOFs is far from being comprehensively explored, and there is considerable untapped potential in this area of research; however, a rigorous approach rooted in the fundamental concepts of solid-state chemistry is needed to fully realise this potential.

To achieve aliovalent substitution, it is crucial to select species that are isomorphous to the original ion, also drawing inspiration from related inorganic materials, where possible. Anticipating and understanding the possible charge compensation mechanisms and their implications for the properties and reactivity of the aliovalent solid solutions of MOFs are other necessary steps, which must start from the accurate determination of the chemical composition. Detailed structural characterisation of these systems is usually made challenging by the difficulty in pinpointing the exact location of the metal species within the framework. Crystallographic techniques can be used to establish the presence of a single crystalline phase. However, the localisation of different metal species is prevented by the intrinsically disordered nature of these systems and requires advanced experimental methods sensitive to the local structure (PDF, EXAFS, SSNMR) and a deep understanding of these techniques to extract meaningful information.

Not all classes of MOFs will be amenable to form aliovalent solid solutions, but with more than 100 000 MOF crystal struc-

tures reported in the Cambridge Structural Database to date, the playing field is huge and there is plenty of room for further investigation. The most obvious step to take is to identify new platforms for aliovalent substitution, possibly expanding the scope to systems other than carboxylate-based MOFs, which have been almost exclusively explored so far. Two examples of phosphonate-based MOFs have been cited here,[142,143] and more could be approached with the same spirit, leveraging the presence of free P–O groups that can be protonated or deprotonated to compensate for excess charges. Moving away from O-donor linkers, azolate-based MOFs are primarily based on soft M^{I}–M^{II} species and are more limited in terms of the aliovalent species to play with, as higher oxidation state metals (*e.g.*, Al^{III}, Fe^{III}, Ti^{IV}, and Zr^{IV}) are predominantly oxophilic. Despite the smaller pool of metals to choose from, the work done with MFU-4*l*, and discussed herein,[47–63] indicates that there is still wide scope to play with similar systems. The so-called anion-pillared MOFs, typically based on neutral N-donor linkers and inorganic anions,[146] are a large class of materials that may also offer interesting opportunities, as aliovalent substitution could be achieved involving not only the metal but also the inorganic anion (*e.g.*, PF_6^-/SiF_6^{2-}).

Understanding how the local structure of the inorganic unit plays a role in determining the range of solid solubility is another area where systematic investigation would be desirable: taking the example of M^{III}-MOFs, it has been highlighted how $[M_3(\mu_3\text{-O})(\text{R-COO})_6(H_2O)_2(OH)]$ SBUs are exceptionally suited as a platform for aliovalent substitution with a wide range of M^{II} and M^{IV}. Does the same hold true also for M^{III}-MOFs containing monodimensional inorganic units, such as MIL-53? More efforts can also be done in terms of incorporating two aliovalent species with different oxidation states within the same inorganic unit, such as M^{II}/M^{IV} in a M^{III}-based MOF or M^{II}/M^{III} in a M^{IV}-based MOF, an area that has been explored to a very limited extent so far[91,92] and could further expand the scope for aliovalent MOFs.

Mastering such fundamental aspects will allow to rationally design aliovalent MOFs with fine-tuned physico-chemical properties for the desired application: the possibility to increase/decrease the availability of Lewis acidic open metal sites *via* aliovalent substitution can be exploited to tune the affinity of the framework for specific guests, a feature of interest for gas/vapour sorption and catalysis. Charge compensation by protonation/deprotonation can alter the Brønsted acidity, affecting catalytic activity and proton conductivity. Similarly, the addition/removal of extraframework ions as a means to compensate excess charges can influence the ion conduction and ion exchange properties. The time is ripe to harness the power of aliovalent substitution in MOFs.

Conflicts of interest

There are no conflicts to declare.

Data availability

No primary research results, software or code have been included, and no new data were generated or analysed as part of this review.

Acknowledgements

Arch. Carla Nicola is acknowledged for hand-drawing the graphical abstract.

References

1 A. R. West, Chapter 2 “Crystal Defects, Non-Stoichiometry and Solid Solutions”, in *Solid State Chemistry and its Applications*, John Wiley & Sons, Ltd, 2nd Edition, 2014.
2 P. M. Woodward, P. Karen, J. S. O. Evans and T. Vogt, Chapter 3 “Defect Chemistry and Nonstoichiometry”, in *Solid State Materials Chemistry*, Cambridge University Press, 2021.
3 P. A. Wright, Chapter 2 “Families of Microporous Framework Solids”, in *Microporous Framework Solids*, Royal Society of Chemistry, 2007.
4 R. P. Townsend and E. N. Coker, Chapter 11 Ion Exchange in Zeolites, in *Studies in Surface Science and Catalysis*, ed. H. van Bekkum, E. M. Flanigen, P. A. Jacobs and J. C. Jansen, Elsevier, 2001, vol. 137, pp. 467–524. DOI: 10.1016/S0167-2991(01)80253-6.
5 E. Pérez-Botella, S. Valencia and F. Rey, Zeolites in Adsorption Processes: State of the Art and Future Prospects, *Chem. Rev*, 2022, 122((24)), 17647–17695. DOI: 10.1021/acs.chemrev.2c00140.
6 T. E. Warner, M. Galsgaard Klokker and U. G. Nielsen, Synthesis and Characterization of Zeolite Na–Y and Its Conversion to the Solid Acid Zeolite H–Y, *J. Chem. Educ.*, 2017, **94**(6), 781–785, DOI: 10.1021/acs.jchemed.6b00718.
7 E. T. C. Vogt and B. M. Weckhuysen, Fluid Catalytic Cracking: Recent Developments on the Grand Old Lady of Zeolite Catalysis, *Chem. Soc. Rev.*, 2015, **44**(20), 7342–7370, DOI: 10.1039/C5CS00376H.
8 G. Mishra, B. Dash and S. Pandey, Layered Double Hydroxides: A Brief Review from Fundamentals to Application as Evolving Biomaterials, *Appl. Clay Sci.*, 2018, **153**, 172–186, DOI: 10.1016/j.clay.2017.12.021.
9 U. Costantino, V. Ambrogi, M. Nocchetti and L. Perioli, Hydrotalcite-like Compounds: Versatile Layered Hosts of Molecular Anions with Biological Activity, *Microporous Mesoporous Mater.*, 2008, **107**(1–2), 149–160, DOI: 10.1016/j.micromeso.2007.02.005.
10 S. Nishimura, A. Takagaki and K. Ebitani, Characterization, Synthesis and Catalysis of Hydrotalcite-Related Materials for Highly Efficient Materials Transformations, *Green Chem.*, 2013, **15**(8), 2026–2042, DOI: 10.1039/C3GC40405F.
11 V. Rives, M. del Arco and C. Martín, Intercalation of Drugs in Layered Double Hydroxides and Their Controlled

Release: A Review, *Appl. Clay Sci.*, 2014, **88–89**, 239–269, DOI: 10.1016/j.clay.2013.12.002.

12 J.-H. Choy, S.-Y. Kwak, J.-S. Park, Y.-J. Jeong and J. Portier, Intercalative Nanohybrids of Nucleoside Monophosphates and DNA in Layered Metal Hydroxide, *J. Am. Chem. Soc.*, 1999, **121**(6), 1399–1400, DOI: 10.1021/ja981823f.

13 A. C. Gomes, S. M. Bruno, C. A. Gamelas, A. A. Valente, M. Abrantes, I. S. Gonçalves, C. C. Romão and M. Pillinger, Intercalation of a Molybdenum H3-Allyl Dicarbonyl Complex in a Layered Double Hydroxide and Catalytic Performance in Olefin Epoxidation, *Dalton Trans.*, 2013, **42**(23), 8231–8240, DOI: 10.1039/C3DT50132A.

14 I. B. Calhau, A. C. Gomes, S. M. Bruno, A. C. Coelho, C. I. R. Magalhães, C. C. Romão, A. A. Valente, I. S. Gonçalves and M. Pillinger, One-Pot Intercalation Strategy for the Encapsulation of a CO-Releasing Organometallic Molecule in a Layered Double Hydroxide, *Eur. J. Inorg. Chem.*, 2020, **2020**(28), 2726–2736, DOI: 10.1002/ejic.202000202.

15 L. Malavasi, C. A. J. Fisher and M. S. Islam, Oxide-Ion and Proton Conducting Electrolyte Materials for Clean Energy Applications: Structural and Mechanistic Features, *Chem. Soc. Rev.*, 2010, **39**(11), 4370–4387, DOI: 10.1039/B915141A.

16 M. Yoshimura, Phase Stability of Zirconia, *Am. Ceram. Soc. Bull.*, 1988, **67**, 1950–1955.

17 M. Mogensen, N. M. Sammes and G. A. Tompsett, Physical, Chemical and Electrochemical Properties of Pure and Doped Ceria, *Solid State Ionics*, 2000, **129**(1), 63–94, DOI: 10.1016/S0167-2738(99)00318-5.

18 M. N. Tsampas, F. M. Sapountzi and P. Vernoux, Applications of Yttria Stabilized Zirconia (YSZ) in Catalysis, *Catal. Sci. Technol.*, 2015, **5**(11), 4884–4900, DOI: 10.1039/C5CY00739A.

19 D.-S. Park, M. Hadad, L. M. Riemer, R. Ignatans, D. Spirito, V. Esposito, V. Tileli, N. Gauquelin, D. Chezganov, D. Jannis, J. Verbeeck, S. Gorfman, N. Pryds, P. Muralt and D. Damjanovic, Induced Giant Piezoelectricity in Centrosymmetric Oxides, *Science*, 2022, **375**(6581), 653–657, DOI: 10.1126/science.abm7497.

20 J. Bitzer and W. Kleist, Synthetic Strategies and Structural Arrangements of Isoreticular Mixed-Component Metal–Organic Frameworks, *Chem. – Eur. J.*, 2019, **25**(8), 1866–1882, DOI: 10.1002/chem.201803887.

21 J. Castells-Gil, N. M. Padial, N. Almora-Barrios, J. Albero, A. R. Ruiz-Salvador, J. González-Platas, H. García and C. Martí-Gastaldo, Chemical Engineering of Photoactivity in Heterometallic Titanium–Organic Frameworks by Metal Doping, *Angew. Chem., Int. Ed.*, 2018, **57**(28), 8453–8457, DOI: 10.1002/anie.201802089.

22 T. Rhauderwiek, H. Zhao, P. Hirschle, M. Döblinger, B. Bueken, H. Reinsch, D. De Vos, S. Wuttke, U. Kolb and N. Stock, Highly Stable and Porous Porphyrin-Based Zirconium and Hafnium Phosphonates – Electron Crystallography as an Important Tool for Structure Elucidation, *Chem. Sci.*, 2018, **9**(24), 5467–5478, DOI: 10.1039/C8SC01533C.

23 X. Song, S. Jeong, D. Kim and M. S. Lah, Transmetalations in Two Metal–Organic Frameworks with Different Framework Flexibilities: Kinetics and Core–Shell Heterostructure, *CrystEngComm*, 2012, **14**(18), 5753–5756, DOI: 10.1039/C2CE26115D.

24 H. Depauw, I. Nevjestić, J. De Winne, G. Wang, K. Haustraete, K. Leus, A. Verberckmoes, C. Detavernier, F. Callens, E. De Canck, H. Vrielinck and P. Van Der Voort, Microwave Induced "Egg Yolk" Structure in Cr/V-MIL-53, *Chem. Commun.*, 2017, **53**(60), 8478–8481, DOI: 10.1039/C7CC04651K.

25 S. Abednatanzi, P. Gohari Derakhshandeh, H. Depauw, F.-X. Coudert, H. Vrielinck, P. Van Der Voort and K. Leus, Mixed-Metal Metal–Organic Frameworks, *Chem. Soc. Rev.*, 2019, **48**(9), 2535–2565, DOI: 10.1039/C8CS00337H.

26 J. Castells-Gil, N. Almora-Barrios, B. Lerma-Berlanga, N. M. Padial and C. Martí-Gastaldo, Chemical Complexity for Targeted Function in Heterometallic Titanium–Organic Frameworks, *Chem. Sci.*, 2023, **14**(25), 6826–6840, DOI: 10.1039/D3SC01550E.

27 M. Y. Masoomi, A. Morsali, A. Dhakshinamoorthy and H. Garcia, Mixed-Metal MOFs: Unique Opportunities in Metal–Organic Framework (MOF) Functionality and Design, *Angew. Chem., Int. Ed.*, 2019, **58**(43), 15188–15205, DOI: 10.1002/anie.201902229.

28 J. A. Botas, G. Calleja, M. Sánchez-Sánchez and M. G. Orcajo, Cobalt Doping of the MOF-5 Framework and Its Effect on Gas-Adsorption Properties, *Langmuir*, 2010, **26**(8), 5300–5303, DOI: 10.1021/la100423a.

29 C. K. Brozek and M. Dincă, Ti3+-, V2+/3+-, Cr2+/3+-, Mn2+-, and Fe2+-Substituted MOF-5 and Redox Reactivity in Cr- and Fe-MOF-5, *J. Am. Chem. Soc.*, 2013, **135**(34), 12886–12891, DOI: 10.1021/ja4064475.

30 P. Guo, C. Froese, Q. Fu, Y.-T. Chen, B. Peng, W. Kleist, R. A. Fischer, M. Muhler and Y. Wang, CuPd Mixed-Metal HKUST-1 as a Catalyst for Aerobic Alcohol Oxidation, *J. Phys. Chem. C*, 2018, **122**(37), 21433–21440, DOI: 10.1021/acs.jpcc.8b05882.

31 W. R. Heinz, T. Kratky, M. Drees, A. Wimmer, O. Tomanec, S. Günther, M. Schuster and R. A. Fischer, Mixed Precious-Group Metal–Organic Frameworks: A Case Study of the HKUST-1 Analogue [RuxRh3−x(BTC)2], *Dalton Trans.*, 2019, **48**(32), 12031–12039, DOI: 10.1039/C9DT01198F.

32 L. J. Wang, H. Deng, H. Furukawa, F. Gándara, K. E. Cordova, D. Peri and O. M. Yaghi, Synthesis and Characterization of Metal–Organic Framework-74 Containing 2, 4, 6, 8, and 10 Different Metals, *Inorg. Chem.*, 2014, **53**(12), 5881–5883, DOI: 10.1021/ic500434a.

33 Y. Jiao, C. R. Morelock, N. C. Burtch, W. P. I. Mounfield, J. T. Hungerford and K. S. Walton, Tuning the Kinetic Water Stability and Adsorption Interactions of Mg-MOF-74 by Partial Substitution with Co or Ni, *Ind. Eng. Chem. Res.*, 2015, **54**(49), 12408–12414, DOI: 10.1021/acs.iecr.5b03843.

34 D. Sun, F. Sun, X. Deng and Z. Li, Mixed-Metal Strategy on Metal–Organic Frameworks (MOFs) for Functionalities Expansion: Co Substitution Induces Aerobic Oxidation of Cyclohexene over Inactive Ni-MOF-74, *Inorg. Chem.*, 2015, **54**(17), 8639–8643, DOI: 10.1021/acs.inorgchem.5b01278.

35 F. Nouar, T. Devic, H. Chevreau, N. Guillou, E. Gibson, G. Clet, M. Daturi, A. Vimont, J. M. Grenèche, M. I. Breeze, R. I. Walton, P. L. Llewellyn and C. Serre, Tuning the Breathing Behaviour of MIL-53 by Cation Mixing, *Chem. Commun.*, 2012, **48**(82), 10237–10239, DOI: 10.1039/C2CC35348B.

36 T. A. Vu, G. H. Le, C. D. Dao, L. Q. Dang, K. T. Nguyen, P. T. Dang, H. T. K. Tran, Q. T. Duong, T. V. Nguyen and G. D. Lee, Isomorphous Substitution of Cr by Fe in MIL-101 Framework and Its Application as a Novel Heterogeneous Photo-Fenton Catalyst for Reactive Dye Degradation, *RSC Adv.*, 2014, **4**(78), 41185–41194, DOI: 10.1039/C4RA06522K.

37 L. Mitchell, P. Williamson, B. Ehrlichová, A. E. Anderson, V. R. Seymour, S. E. Ashbrook, N. Acerbi, L. M. Daniels, R. I. Walton, M. L. Clarke and P. A. Wright, Mixed-Metal MIL-100(Sc,M) (M=Al, Cr, Fe) for Lewis Acid Catalysis and Tandem C-C Bond Formation and Alcohol Oxidation, *Chem. – Eur. J.*, 2014, **20**(51), 17185–17197, DOI: 10.1002/chem.201404377.

38 M. Lammert, C. Glißmann and N. Stock, Tuning the Stability of Bimetallic Ce(Iv)/Zr(Iv)-Based MOFs with UiO-66 and MOF-808 Structures, *Dalton Trans.*, 2017, **46**(8), 2425–2429, DOI: 10.1039/C7DT00259A.

39 C. Atzori, K. A. Lomachenko, J. Jacobsen, N. Stock, A. Damin, F. Bonino and S. Bordiga, Bimetallic Hexanuclear Clusters in Ce/Zr-UiO-66 MOFs: In Situ FTIR Spectroscopy and Modelling Insights, *Dalton Trans.*, 2020, **49**(18), 5794–5797, DOI: 10.1039/D0DT01023E.

40 K. A. Lomachenko, J. Jacobsen, A. L. Bugaev, C. Atzori, F. Bonino, S. Bordiga, N. Stock and C. Lamberti, Exact Stoichiometry of CexZr6−x Cornerstones in Mixed-Metal UiO-66 Metal–Organic Frameworks Revealed by Extended X-Ray Absorption Fine Structure Spectroscopy, *J. Am. Chem. Soc.*, 2018, **140**(50), 17379–17383, DOI: 10.1021/jacs.8b10343.

41 C. K. Brozek and M. Dincă, Cation Exchange at the Secondary Building Units of Metal–Organic Frameworks, *Chem. Soc. Rev.*, 2014, **43**(16), 5456–5467, DOI: 10.1039/C4CS00002A.

42 R. D. Shannon, Revised Effective Ionic Radii and Systematic Studies of Interatomic Distances in Halides and Chalcogenides, *Acta Crystallogr., Sect. A: Found. Crystallogr.*, 1976, **32**(5), 751–767, DOI: 10.1107/S0567739476001551.

43 S. Das, H. Kim and K. Kim, Metathesis in Single Crystal: Complete and Reversible Exchange of Metal Ions Constituting the Frameworks of Metal–Organic Frameworks, *J. Am. Chem. Soc.*, 2009, **131**(11), 3814–3815, DOI: 10.1021/ja808995d.

44 Y. Kim, S. Das, S. Bhattacharya, S. Hong, M. G. Kim, M. Yoon, S. Natarajan and K. Kim, Metal-Ion Metathesis in Metal–Organic Frameworks: A Synthetic Route to New Metal–Organic Frameworks, *Chem. – Eur. J.*, 2012, **18**(52), 16642–16648, DOI: 10.1002/chem.201202899.

45 N. M. Padial, B. Lerma-Berlanga, N. Almora-Barrios, J. Castells-Gil, I. da Silva, M. de la Mata, S. I. Molina, J. Hernández-Saz, A. E. Platero-Prats, S. Tatay and C. Martí-Gastaldo, Heterometallic Titanium–Organic Frameworks by Metal-Induced Dynamic Topological Transformations, *J. Am. Chem. Soc.*, 2020, **142**(14), 6638–6648, DOI: 10.1021/jacs.0c00117.

46 V. Rubio-Giménez, J. C. Waerenborgh, J. M. Clemente-Juan and C. Martí-Gastaldo, Spontaneous Magnetization in Heterometallic NiFe-MOF-74 Microporous Magnets by Controlled Iron Doping, *Chem. Mater.*, 2017, **29**(15), 6181–6185, DOI: 10.1021/acs.chemmater.7b01601.

47 D. Denysenko, M. Grzywa, M. Tonigold, B. Streppel, I. Krkljus, M. Hirscher, E. Mugnaioli, U. Kolb, J. Hanss and D. Volkmer, Elucidating Gating Effects for Hydrogen Sorption in MFU-4-Type Triazolate-Based Metal–Organic Frameworks Featuring Different Pore Sizes, *Chem. – Eur. J.*, 2011, **17**(6), 1837–1848, DOI: 10.1002/chem.201001872.

48 D. Denysenko, M. Grzywa, J. Jelic, K. Reuter and D. Volkmer, Scorpionate-Type Coordination in MFU-4 l Metal–Organic Frameworks: Small-Molecule Binding and Activation upon the Thermally Activated Formation of Open Metal Sites, *Angew. Chem., Int. Ed.*, 2014, **53**(23), 5832–5836, DOI: 10.1002/anie.201310004.

49 D. Denysenko, J. Jelic, O. V. Magdysyuk, K. Reuter and D. Volkmer, Elucidating Lewis Acidity of Metal Sites in MFU-4 l Metal-Organic Frameworks: N2O and CO2 Adsorption in MFU-4 l, CuI-MFU-4 l and Li-MFU-4 l, *Microporous Mesoporous Mater.*, 2015, **216**, 146–150, DOI: 10.1016/j.micromeso.2015.03.014.

50 I. Weinrauch, I. Savchenko, D. Denysenko, S. M. Souliou, H.-H. Kim, M. Le Tacon, L. L. Daemen, Y. Cheng, A. Mavrandonakis, A. J. Ramirez-Cuesta, D. Volkmer, G. Schütz, M. Hirscher and T. Heine, Capture of Heavy Hydrogen Isotopes in a Metal-Organic Framework with Active Cu(I) Sites, *Nat. Commun.*, 2017, **8**(1), 14496, DOI: 10.1038/ncomms14496.

51 S. A. FitzGerald, D. Mukasa, K. H. Rigdon, N. Zhang and B. R. Barnett, Hydrogen Isotope Separation within the Metal–Organic Framework Cu(I)-MFU-4 l, *J. Phys. Chem. C*, 2019, **123**(50), 30427–30433, DOI: 10.1021/acs.jpcc.9b09332.

52 M. H. Mohamed, Y. Yang, L. Li, S. Zhang, J. P. Ruffley, A. G. Jarvi, S. Saxena, G. Veser, J. K. Johnson and N. L. Rosi, Designing Open Metal Sites in Metal–Organic Frameworks for Paraffin/Olefin Separations, *J. Am. Chem. Soc.*, 2019, **141**(33), 13003–13007, DOI: 10.1021/jacs.9b06582.

53 L. Li, Y. Yang, M. H. Mohamed, S. Zhang, G. Veser, N. L. Rosi and J. K. Johnson, Fundamental Insights into the Reactivity and Utilization of Open Metal Sites in Cu(I)-MFU-4 l, *Organometallics*, 2019, **38**(18), 3453–3459, DOI: 10.1021/acs.organomet.9b00351.

54 H.-L. Zhu, J.-R. Huang, X.-W. Zhang, C. Wang, N.-Y. Huang, P.-Q. Liao and X.-M. Chen, Highly Efficient Electroconversion of CO2 into CH4 by a Metal–Organic Framework with Trigonal Pyramidal Cu(I)N3 Active Sites, *ACS Catal.*, 2021, **11**(18), 11786–11792, DOI: 10.1021/acscatal.1c02980.

55 Z. Chen, M. R. Mian, S.-J. Lee, H. Chen, X. Zhang, K. O. Kirlikovali, S. Shulda, P. Melix, A. S. Rosen, P. A. Parilla, T. Gennett, R. Q. Snurr, T. Islamoglu, T. Yildirim and O. K. Farha, Fine-Tuning a Robust Metal–Organic Framework toward Enhanced Clean Energy Gas Storage, *J. Am. Chem. Soc.*, 2021, **143**(45), 18838–18843, DOI: 10.1021/jacs.1c08749.

56 G. M. Su, H. Wang, B. R. Barnett, J. R. Long, D. Prendergast and W. S. Drisdell, Backbonding Contributions to Small Molecule Chemisorption in a Metal–Organic Framework with Open Copper(I) Centers, *Chem. Sci.*, 2021, **12**(6), 2156–2164, DOI: 10.1039/D0SC06038K.

57 L. M. Funke, R. Chakraborty, K. M. Carsch, M. Head-Gordon, J. R. Long and J. A. Reimer, Assessment of Adsorbate π-Backbonding in Copper(I) Metal–Organic Frameworks via Multinuclear NMR Spectroscopy and Density Functional Theory Calculations, *J. Phys. Chem. C*, 2023, **127**(15), 7513–7519, DOI: 10.1021/acs.jpcc.3c00462.

58 Y. Yabuuchi, H. Furukawa, K. M. Carsch, R. A. Klein, N. V. Tkachenko, A. J. Huang, Y. Cheng, K. M. Taddei, E. Novak, C. M. Brown, M. Head-Gordon and J. R. Long, Geometric Tuning of Coordinatively Unsaturated Copper (I) Sites in Metal–Organic Frameworks for Ambient-Temperature Hydrogen Storage, *J. Am. Chem. Soc.*, 2024, **146**(32), 22759–22776, DOI: 10.1021/jacs.4c08039.

59 T. Pan, K. Yang, X. Dong, J. Tao and Y. Han, Creating Cu(I) Sites in an MOF for Reversible Capture of Molecular Iodine at Low Concentrations and High Temperatures, *ACS Mater. Lett.*, 2024, **6**(7), 2794–2801, DOI: 10.1021/acsmaterialslett.4c00625.

60 K. M. Carsch, A. J. Huang, M. N. Dods, S. T. Parker, R. C. Rohde, H. Z. H. Jiang, Y. Yabuuchi, S. L. Karstens, H. Kwon, R. Chakraborty, K. C. Bustillo, K. R. Meihaus, H. Furukawa, A. M. Minor, M. Head-Gordon and J. R. Long, Selective Adsorption of Oxygen from Humid Air in a Metal–Organic Framework with Trigonal Pyramidal Copper(I) Sites, *J. Am. Chem. Soc.*, 2024, **146**(5), 3160–3170, DOI: 10.1021/jacs.3c10753.

61 N. V. Tkachenko, Y. Yabuuchi, K. M. Carsch, H. Furukawa, J. R. Long and M. Head-Gordon, Computational Optimization of Room Temperature Usable Capacity for Hydrogen Storage in MFU-4-Type Metal–Organic Frameworks via Pairwise Metal Substitutions, *J. Phys. Chem. C*, 2025, **129**(1), 167–178, DOI: 10.1021/acs.jpcc.4c07631.

62 F. Zhang, Z. Zhao, Y. Wang, X. Li, X. Bai, M. Lu, Y. Wang, X. Wang, L. Li, J. Li and J. Yang, Nitrogen Adsorption Sites with Low Polarizability for Benchmark N_2/CH_4 Separation, *Angew. Chem., Int. Ed.*, 2025, **64**(36), e202510242, DOI: 10.1002/anie.202510242.

63 H. D. Park, R. J. Comito, Z. Wu, G. Zhang, N. Ricke, C. Sun, T. Van Voorhis, J. T. Miller, Y. Román-Leshkov and M. Dincă, Gas-Phase Ethylene Polymerization by Single-Site Cr Centers in a Metal–Organic Framework, *ACS Catal.*, 2020, **10**(6), 3864–3870, DOI: 10.1021/acscatal.9b03282.

64 D. Feng, K. Wang, Z. Wei, Y.-P. Chen, C. M. Simon, R. K. Arvapally, R. L. Martin, M. Bosch, T.-F. Liu, S. Fordham, D. Yuan, M. A. Omary, M. Haranczyk, B. Smit and H.-C. Zhou, Kinetically Tuned Dimensional Augmentation as a Versatile Synthetic Route towards Robust Metal–Organic Frameworks, *Nat. Commun.*, 2014, **5**(1), 5723, DOI: 10.1038/ncomms6723.

65 S. Wongsakulphasatch, F. Nouar, J. Rodriguez, L. Scott, C. Le Guillouzer, T. Devic, P. Horcajada, J.-M. Grenèche, P. L. Llewellyn, A. Vimont, G. Clet, M. Daturi and C. Serre, Direct Accessibility of Mixed-Metal (Iii/Ii) Acid Sites through the Rational Synthesis of Porous Metal Carboxylates, *Chem. Commun.*, 2015, **51**(50), 10194–10197, DOI: 10.1039/C5CC02550H.

66 Q.-G. Zhai, X. Bu, C. Mao, X. Zhao and P. Feng, Systematic and Dramatic Tuning on Gas Sorption Performance in Heterometallic Metal–Organic Frameworks, *J. Am. Chem. Soc.*, 2016, **138**(8), 2524–2527, DOI: 10.1021/jacs.5b13491.

67 Y. Chen, Z. Qiao, J. Huang, H. Wu, J. Xiao, Q. Xia, H. Xi, J. Hu, J. Zhou and Z. Li, Unusual Moisture-Enhanced CO2 Capture within Microporous PCN-250 Frameworks, *ACS Appl. Mater. Interfaces*, 2018, **10**(44), 38638–38647, DOI: 10.1021/acsami.8b14400.

68 M. Giménez-Marqués, A. Santiago-Portillo, S. Navalón, M. Álvaro, V. Briois, F. Nouar, H. Garcia and C. Serre, Exploring the Catalytic Performance of a Series of Bimetallic MIL-100(Fe, Ni) MOFs, *J. Mater. Chem. A*, 2019, **7**(35), 20285–20292, DOI: 10.1039/C9TA01948K.

69 Y. Gu, D. Xie, Y. Wang, W. Qin, H. Zhang, G. Wang, Y. Zhang and H. Zhao, Facile Fabrication of Composition-Tunable Fe/Mg Bimetal-Organic Frameworks for Exceptional Arsenate Removal, *Chem. Eng. J.*, 2019, **357**, 579–588, DOI: 10.1016/j.cej.2018.09.174.

70 T. Steenhaut, S. Hermans and Y. Filinchuk, Green Synthesis of a Large Series of Bimetallic MIL-100(Fe,M) MOFs, *New J. Chem.*, 2020, **44**(10), 3847–3855, DOI: 10.1039/D0NJ00257G.

71 A. Kirchon, P. Zhang, J. Li, E. A. Joseph, W. Chen and H.-C. Zhou, Effect of Isomorphic Metal Substitution on the Fenton and Photo-Fenton Degradation of Methylene Blue Using Fe-Based Metal–Organic Frameworks, *ACS Appl. Mater. Interfaces*, 2020, **12**(8), 9292–9299, DOI: 10.1021/acsami.9b21408.

72 H. F. Drake, Z. Xiao, G. S. Day, S. W. Vali, W. Chen, Q. Wang, Y. Huang, T.-H. Yan, J. E. Kuszynski, P. A. Lindahl, M. R. Ryder and H.-C. Zhou, Thermal Decarboxylation for the Generation of Hierarchical Porosity in Isostructural Metal–Organic Frameworks Containing Open Metal Sites, *Mater. Adv.*, 2021, **2**(16), 5487–5493, DOI: 10.1039/D1MA00163A.

73 T. H. Rupam, T. Steenhaut, M. L. Palash, Y. Filinchuk, S. Hermans and B. B. Saha, Thermochemical Energy Applications of Green Transition Metal Doped MIL–100 (Fe), *Chem. Eng. J.*, 2022, **448**, 137590, DOI: 10.1016/j.cej.2022.137590.

74 W. Chen, Z. Wang, Q. Wang, K. El-Yanboui, K. Tan, H. M. Barkholtz, D.-J. Liu, P. Cai, L. Feng, Y. Li, J.-S. Qin, S. Yuan, D. Sun and H.-C. Zhou, Monitoring the Activation of Open Metal Sites in $[Fe_xM_{3-x}(\mu_3\text{-}O)]$ Cluster-Based Metal–Organic Frameworks by Single-Crystal X-Ray Diffraction, *J. Am. Chem. Soc.*, 2023, **145**(8), 4736–4745, DOI: 10.1021/jacs.2c13299.

75 B. Yeh, S. Chheda, S. D. Prinslow, A. S. Hoffman, J. Hong, J. E. Perez-Aguilar, S. R. Bare, C. C. Lu, L. Gagliardi and A. Bhan, Structure and Site Evolution of Framework Ni Species in MIL-127 MOFs for Propylene Oligomerization Catalysis, *J. Am. Chem. Soc.*, 2023, **145**(6), 3408–3418, DOI: 10.1021/jacs.2c10551.

76 J. Catterick and P. Thornton, Structures and Physical Properties of Polynuclear Carboxylates, in *Advances in Inorganic Chemistry and Radiochemistry*, ed. H. J. Emeléus and A. G. Sharpe, Academic Press, 1977, vol. 20, pp. 291–362. DOI: 10.1016/S0065-2792(08)60041-2.

77 F. A. Cotton and J. G. Norman, Structural Characterization of a Basic Trinuclear Ruthenium Acetate, *Inorg. Chim. Acta*, 1972, 6, 411–419. DOI: 10.1016/S0020-1693(00)91829-2.

78 D. Lupu, D. Barb, G. Filoti, M. Morariu and D. Tarină, Mössbauer Spectra and Thermal Electron Transfer in Mixed Valence Iron Compounds, *J. Inorg. Nucl. Chem.*, 1972, **34**(9), 2803–2810, DOI: 10.1016/0022-1902(72)80585-2.

79 F. A. Cotton and W. Wang, New Trinuclear, Oxo-Centered, Basic Carboxylate Compounds of Transition Metals. 1. Trichromium(II,III,III) Compounds, *Inorg. Chem.*, 1982, **21**(7), 2675–2678, DOI: 10.1021/ic00137a028.

80 F. A. Cotton, G. E. Lewis and G. N. Mott, New Trinuclear, Oxo-Centered, Basic Carboxylate Compounds of Transition Metals. 3. Syntheses and x-Ray Studies of the Trivanadium(III,III,III) and Trivanadium(II,III,III) Compounds [V3(.Mu.3-O)(CH_3CO2)6(CH_3COOH)2(THF)] + [VCl4(CH_3COOH)2]- and V3(.Mu.3-O)(CF3CO2)6(THF)3 with "Classical" Triangular Structures, *Inorg. Chem.*, 1982, **21**(9), 3316–3321, DOI: 10.1021/ic00139a013.

81 R. Weinland and H. Holtmeier, Über Ferri-Nickel- Usw. -Acetate Und Über Ein Sehr Basisches Kristallisiertes Ferriacetat, *Z. Anorg. Allg. Chem.*, 1928, **173**(1), 49–62, DOI: 10.1002/zaac.19281730106.

82 A. B. Blake, A. Yavari and H. Kubicki, Exchange Interactions in a Series of Novel Heteronuclear Basic Carboxylate Complexes Containing Two Iron(III) Ions and a Divalent Metal Ion, *J. Chem. Soc., Chem. Commun.*, 1981, (15), 796–797, DOI: 10.1039/C39810000796.

83 A. B. Blake, A. Yavari, W. E. Hatfield and C. N. Sethulekshmi, Magnetic and Spectroscopic Properties of Some Heterotrinuclear Basic Acetates of Chromium(III), Iron(III), and Divalent Metal Ions, *J. Chem. Soc., Dalton Trans.*, 1985, (12), 2509–2520, DOI: 10.1039/DT9850002509.

84 Y. Liu, J. F. Eubank, A. J. Cairns, J. Eckert, V. C. Kravtsov, R. Luebke and M. Eddaoudi, Assembly of Metal–Organic Frameworks (MOFs) Based on Indium-Trimer Building Blocks: A Porous MOF with Soc Topology and High Hydrogen Storage, *Angew. Chem., Int. Ed.*, 2007, **46**(18), 3278–3283, DOI: 10.1002/anie.200604306.

85 A. Dhakshinamoorthy, M. Alvaro, H. Chevreau, P. Horcajada, T. Devic, C. Serre and H. Garcia, Iron(III) Metal–Organic Frameworks as Solid Lewis Acids for the Isomerization of α-Pinene Oxide, *Catal. Sci. Technol.*, 2012, **2**(2), 324–330, DOI: 10.1039/C2CY00376G.

86 Q.-G. Zhai, X. Bu, C. Mao, X. Zhao and P. Feng, Systematic and Dramatic Tuning on Gas Sorption Performance in Heterometallic Metal–Organic Frameworks, *J. Am. Chem. Soc.*, 2016, **138**(8), 2524–2527, DOI: 10.1021/jacs.5b13491.

87 B. Bueken, F. Vermoortele, D. E. P. Vanpoucke, H. Reinsch, C.-C. Tsou, P. Valvekens, T. De Baerdemaeker, R. Ameloot, C. E. A. Kirschhock, V. Van Speybroeck, J. M. Mayer and D. A. De Vos, Flexible Photoactive Titanium Metal–Organic Framework Based on a [TiIV3(M3-O)(O)2(COO)6] Cluster, *Angew. Chem., Int. Ed.*, 2015, **54**(47), 13912–13917, DOI: 10.1002/anie.201505512.

88 J. Castells-Gil, N. M. Padial, N. Almora-Barrios, I. d. Silva, D. Mateo, J. Albero, H. García and C. Martí-Gastaldo, De Novo Synthesis of Mesoporous Photoactive Titanium(IV)–Organic Frameworks with MIL-100 Topology, *Chem. Sci.*, 2019, **10**(15), 4313–4321, DOI: 10.1039/C8SC05218B.

89 H. Gao, L. Yu, J. Zhang, J.-P. Gao and X.-M. Zhang, High Proton Conduction for CPM-200 Achieved by Aliovalent-Predefinition of $M_3(\mu_3\text{-}O)$ Building Blocks and In Situ Encapsulation of Hydrated Metal Ions, *ACS Mater. Lett.*, 2024, **6**(3), 765–771, DOI: 10.1021/acsmaterialslett.3c01552.

90 A. L. Spek, Single-Crystal Structure Validation with the Program It PLATON, *J. Appl. Crystallogr.*, 2003, **36**(1), 7–13, DOI: 10.1107/S0021889802022112.

91 K. Hong, W. Bak, D. Moon and H. Chun, Bistable and Porous Metal–Organic Frameworks with Charge-Neutral Acs Net Based on Heterometallic $M_3O(CO_2)_6$ Building Blocks, *Cryst. Growth Des.*, 2013, **13**(9), 4066–4070, DOI: 10.1021/cg4009009.

92 J. Castells-Gil, N. M. Padial, N. Almora-Barrios, R. Gil-San-Millán, M. Romero-Ángel, V. Torres, I. da Silva, B. C. J. Vieira, J. C. Waerenborgh, J. Jagiello, J. A. R. Navarro, S. Tatay and C. Martí-Gastaldo, Heterometallic Titanium-Organic Frameworks as Dual-Metal Catalysts for Synergistic Non-Buffered Hydrolysis of Nerve Agent Simulants, *Chem*, 2020, **6**(11), 3118–3131, DOI: 10.1016/j.chempr.2020.09.002.

93 A. Rubio-Gaspar, S. Navalón, S. Tatay, F. G. Cirujano, C. Fernández-Conde, N. M. Padial and C. Martí-Gastaldo, Metal Node Control of Brønsted Acidity in

Heterobimetallic Titanium–Organic Frameworks, *J. Am. Chem. Soc.*, 2023, **145**(7), 3855–3860, DOI: 10.1021/jacs.2c12718.

94 J. Castells-Gil, S. Ould-Chikh, A. Ramírez, R. Ahmad, G. Prieto, A. R. Gómez, L. Garzón-Tovar, S. Telalovic, L. Liu, A. Genovese, N. M. Padial, A. Aguilar-Tapia, P. Bordet, L. Cavallo, C. Martí-Gastaldo and J. Gascon, Unlocking Mixed Oxides with Unprecedented Stoichiometries from Heterometallic Metal-Organic Frameworks for the Catalytic Hydrogenation of CO2, *Chem. Catal.*, 2021, **1**(2), 364–382, DOI: 10.1016/j.checat.2021.03.010.

95 N. M. Padial, B. Lerma-Berlanga, N. Almora-Barrios, J. Castells-Gil, I. da Silva, M. de la Mata, S. I. Molina, J. Hernández-Saz, A. E. Platero-Prats, S. Tatay and C. Martí-Gastaldo, Heterometallic Titanium–Organic Frameworks by Metal-Induced Dynamic Topological Transformations, *J. Am. Chem. Soc.*, 2020, **142**(14), 6638–6648, DOI: 10.1021/jacs.0c00117.

96 E. P. Gómez-Oliveira, J. Castells-Gil, C. Chinchilla-Garzón, A. Uscategui-Linares, J. Albero, N. Almora-Barrios, S. Tatay, N. M. Padial and C. Martí-Gastaldo, Integrating Compositional and Structural Diversity in Heterometallic Titanium Frameworks by Metal Exchange Methods, *J. Am. Chem. Soc.*, 2024, **146**(45), 31021–31033, DOI: 10.1021/jacs.4c10444.

97 O. Kozachuk, M. Meilikhov, K. Yusenko, A. Schneemann, B. Jee, A. V. Kuttatheyil, M. Bertmer, C. Sternemann, A. Pöppl and R. A. Fischer, A Solid-Solution Approach to Mixed-Metal Metal–Organic Frameworks – Detailed Characterization of Local Structures, Defects and Breathing Behaviour of Al/V Frameworks, *Eur. J. Inorg. Chem.*, 2013, **2013**(26), 4546–4557, DOI: 10.1002/ejic.201300591.

98 H. Depauw, I. Nevjestić, G. Wang, K. Leus, F. Callens, E. De Canck, K. De Buysser, H. Vrielinck and P. Van Der Voort, Discovery of a Novel, Large Pore Phase in a Bimetallic Al/V Metal–Organic Framework, *J. Mater. Chem. A*, 2017, **5**(47), 24580–24584, DOI: 10.1039/C7TA08103K.

99 I. Nevjestić, H. Depauw, K. Leus, V. Kalendra, I. Caretti, G. Jeschke, S. Van Doorslaer, F. Callens, P. Van Der Voort and H. Vrielinck, Multi-Frequency (S, X, Q and W-Band) EPR and ENDOR Study of Vanadium(IV) Incorporation in the Aluminium Metal–Organic Framework MIL-53, *ChemPhysChem*, 2015, **16**(14), 2968–2973, DOI: 10.1002/cphc.201500522.

100 I. Nevjestić, H. Depauw, K. Leus, G. Rampelberg, C. A. Murray, C. Detavernier, P. Van Der Voort, F. Callens and H. Vrielinck, In Situ Electron Paramagnetic Resonance and X-Ray Diffraction Monitoring of Temperature-Induced Breathing and Related Structural Transformations in Activated V-Doped MIL-53(Al), *J. Phys. Chem. C*, 2016, **120**(31), 17400–17407, DOI: 10.1021/acs.jpcc.6b04402.

101 I. Nevjestić, H. Depauw, P. Gast, P. Tack, D. Deduytsche, K. Leus, M. Van Landeghem, E. Goovaerts, L. Vincze, C. Detavernier, P. Van Der Voort, F. Callens and H. Vrielinck, Sensing the Framework State and Guest Molecules in MIL-53(Al) via the Electron Paramagnetic Resonance Spectrum of VIV Dopant Ions, *Phys. Chem. Chem. Phys.*, 2017, **19**(36), 24545–24554, DOI: 10.1039/C7CP04760F.

102 K. Maes, L. I. D. J. Martin, S. Khelifi, A. Hoffman, K. Leus, P. Van Der Voort, E. Goovaerts, P. F. Smet, V. Van Speybroeck, F. Callens and H. Vrielinck, Identification of Vanadium Dopant Sites in the Metal–Organic Framework DUT-5(Al), *Phys. Chem. Chem. Phys.*, 2021, **23**(12), 7088–7100, DOI: 10.1039/D1CP00695A.

103 S. Yang, J. Sun, A. J. Ramirez-Cuesta, S. K. Callear, W. I. F. David, D. P. Anderson, R. Newby, A. J. Blake, J. E. Parker, C. C. Tang and M. Schröder, Selectivity and Direct Visualization of Carbon Dioxide and Sulfur Dioxide in a Decorated Porous Host, *Nat. Chem.*, 2012, **4**(11), 887–894, DOI: 10.1038/nchem.1457.

104 H. Gao, Y.-B. He, J.-J. Hou and X.-M. Zhang, In Situ Aliovalent Nickle Substitution and Acidic Modification of Nanowalls Promoted Proton Conductivity in InOF with 1D Helical Channel, *ACS Appl. Mater. Interfaces*, 2021, **13**(32), 38289–38295, DOI: 10.1021/acsami.1c09001.

105 H. Gao, Y.-B. He, J.-J. Hou, Q.-G. Zhai and X.-M. Zhang, Enhanced Proton Conductivity by Aliovalent Substitution of Cadmium for Indium in Dimethylaminium-Templated Metal Anilicates, *ACS Appl. Mater. Interfaces*, 2020, **12**(37), 41605–41612, DOI: 10.1021/acsami.0c13125.

106 H. Gao, Y.-X. Wang, Y.-B. He and X.-M. Zhang, Sequential Enhancement of Proton Conductivity by Aliovalent Cadmium Substitution and Post-Synthetic Esterolysis in a Carboxylate-Functionalized Indium Framework with Dimethylaminium Templates, *Inorg. Chem. Front.*, 2022, **9**(12), 2997–3002, DOI: 10.1039/D2QI00407K.

107 L. Wang, A. Daru, B. Jangid, J.-H. Chen, N. Jiang, S. N. Patel, L. Gagliardi and J. S. Anderson, Aliovalent Substitution Tunes Physical Properties in a Conductive Bis(Dithiolene) Two-Dimensional Metal–Organic Framework, *J. Am. Chem. Soc.*, 2024, **146**(17), 12063–12073, DOI: 10.1021/jacs.4c01860.

108 J. H. Cavka, S. Jakobsen, U. Olsbye, N. Guillou, C. Lamberti, S. Bordiga and K. P. Lillerud, A New Zirconium Inorganic Building Brick Forming Metal Organic Frameworks with Exceptional Stability, *J. Am. Chem. Soc.*, 2008, **130**(42), 13850–13851, DOI: 10.1021/ja8057953.

109 Y. Bai, Y. Dou, L.-H. Xie, W. Rutledge, J.-R. Li and H.-C. Zhou, Zr-Based Metal–Organic Frameworks: Design, Synthesis, Structure, and Applications, *Chem. Soc. Rev.*, 2016, **45**(8), 2327–2367, DOI: 10.1039/C5CS00837A.

110 J. Jacobsen, A. Ienco, R. D'Amato, F. Costantino and N. Stock, The Chemistry of Ce-Based Metal–Organic Frameworks, *Dalton Trans.*, 2020, **49**(46), 16551–16586, DOI: 10.1039/D0DT02813D.

111 K. E. deKrafft, W. S. Boyle, L. M. Burk, O. Z. Zhou and W. Lin, Zr- and Hf-Based Nanoscale Metal–Organic

Frameworks as Contrast Agents for Computed Tomography, *J. Mater. Chem.*, 2012, **22**(35), 18139–18144, DOI: 10.1039/C2JM32299D.

112 C. Falaise, J.-S. Charles, C. Volkringer and T. Loiseau, Thorium Terephthalates Coordination Polymers Synthesized in Solvothermal DMF/H_2O System, *Inorg. Chem.*, 2015, **54**(5), 2235–2242, DOI: 10.1021/ic502725y.

113 C. Falaise, C. Volkringer, J.-F. Vigier, N. Henry, A. Beaurain and T. Loiseau, Three-Dimensional MOF-Type Architectures with Tetravalent Uranium Hexanuclear Motifs (U6O8), *Chem. – Eur. J.*, 2013, **19**(17), 5324–5331, DOI: 10.1002/chem.201203914.

114 A. M. Hastings, D. Ray, W. Jeong, L. Gagliardi, O. K. Farha and A. E. Hixon, Advancement of Actinide Metal–Organic Framework Chemistry via Synthesis of Pu-UiO-66, *J. Am. Chem. Soc.*, 2020, **142**(20), 9363–9371, DOI: 10.1021/jacs.0c01895.

115 M. J. Cliffe, E. Castillo-Martínez, Y. Wu, J. Lee, A. C. Forse, F. C. N. Firth, P. Z. Moghadam, D. Fairen-Jimenez, M. W. Gaultois, J. A. Hill, O. V. Magdysyuk, B. Slater, A. L. Goodwin and C. P. Grey, Metal–Organic Nanosheets Formed via Defect-Mediated Transformation of a Hafnium Metal–Organic Framework, *J. Am. Chem. Soc.*, 2017, **139**(15), 5397–5404, DOI: 10.1021/jacs.7b00106.

116 S. Leubner, H. Zhao, N. Van Velthoven, M. Henrion, H. Reinsch, D. E. De Vos, U. Kolb and N. Stock, Expanding the Variety of Zirconium-Based Inorganic Building Units for Metal–Organic Frameworks, *Angew. Chem., Int. Ed.*, 2019, **58**(32), 10995–11000, DOI: 10.1002/anie.201905456.

117 H. G. Scott, Phase Relationships in the Zirconia-Yttria System, *J. Mater. Sci.*, 1975, **10**(9), 1527–1535, DOI: 10.1007/BF01031853.

118 D.-X. Xue, A. J. Cairns, Y. Belmabkhout, L. Wojtas, Y. Liu, M. H. Alkordi and M. Eddaoudi, Tunable Rare-Earth Fcu-MOFs: A Platform for Systematic Enhancement of CO_2 Adsorption Energetics and Uptake, *J. Am. Chem. Soc.*, 2013, **135**(20), 7660–7667, DOI: 10.1021/ja401429x.

119 F. Saraci, V. Quezada-Novoa, P. R. Donnarumma and A. J. Howarth, Rare-Earth Metal–Organic Frameworks: From Structure to Applications, *Chem. Soc. Rev.*, 2020, **49**(22), 7949–7977, DOI: 10.1039/D0CS00292E.

120 J. P. Vizuet, M. L. Mortensen, A. L. Lewis, M. A. Wunch, H. R. Firouzi, G. T. McCandless and K. J. Jr. Balkus, Fluoro-Bridged Clusters in Rare-Earth Metal–Organic Frameworks, *J. Am. Chem. Soc.*, 2021, **143**(43), 17995–18000, DOI: 10.1021/jacs.1c10493.

121 M. Abbas, S. Sheybani, M. L. Mortensen and K. J. Balkus, Fluoro-Bridged Rare-Earth Metal–Organic Frameworks, *Dalton Trans.*, 2024, **53**(8), 3445–3453, DOI: 10.1039/D3DT03814A.

122 A. M. Ebrahim and T. J. Bandosz, Ce(III) Doped Zr-Based MOFs as Excellent NO2 Adsorbents at Ambient Conditions, *ACS Appl. Mater. Interfaces*, 2013, **5**(21), 10565–10573, DOI: 10.1021/am402305u.

123 Z. Yue, S. Liu and Y. Liu, Yttria Stabilized Zirconia Derived from Metal–Organic Frameworks, *RSC Adv.*, 2015, **5**(14), 10619–10622, DOI: 10.1039/C4RA14728F.

124 J. Feng, T. Liu, J. Shi, S. Gao and R. Cao, Dual-Emitting UiO-66(Zr&Eu) Metal–Organic Framework Films for Ratiometric Temperature Sensing, *ACS Appl. Mater. Interfaces*, 2018, **10**(24), 20854–20861, DOI: 10.1021/acsami.8b04889.

125 M. A. Syzgantseva, C. P. Ireland, F. M. Ebrahim, B. Smit and O. A. Syzgantseva, Metal Substitution as the Method of Modifying Electronic Structure of Metal–Organic Frameworks, *J. Am. Chem. Soc.*, 2019, **141**(15), 6271–6278, DOI: 10.1021/jacs.8b13667.

126 R. Gil-San-Millan, E. López-Maya, A. E. Platero-Prats, V. Torres-Pérez, P. Delgado, A. W. Augustyniak, M. K. Kim, H. W. Lee, S. G. Ryu and J. A. R. Navarro, Magnesium Exchanged Zirconium Metal–Organic Frameworks with Improved Detoxification Properties of Nerve Agents, *J. Am. Chem. Soc.*, 2019, **141**(30), 11801–11805, DOI: 10.1021/jacs.9b05571.

127 R. Qin and H. C. Zeng, Confined Transformation of UiO–66 Nanocrystals to Yttria–Stabilized Zirconia with Hierarchical Pore Structures for Catalytic Applications, *Adv. Funct. Mater.*, 2019, **29**(39), 1903264, DOI: 10.1002/adfm.201903264.

128 X. Kong, Q. Pan, S. Song, Z. He, T. Zeng and Y. Yu, Dual Metal UiO-Type Metal–Organic Frameworks for Solar-Driven Photocatalytic Hydrogen Evolution, *J. Phys. Chem. C*, 2021, **125**(37), 20320–20330, DOI: 10.1021/acs.jpcc.1c05866.

129 M. Ronda-Lloret, I. Pellicer-Carreño, A. Grau-Atienza, R. Boada, S. Diaz-Moreno, J. Narciso-Romero, J. C. Serrano-Ruiz, A. Sepúlveda-Escribano and E. V. Ramos-Fernandez, Mixed-Valence Ce/Zr Metal-Organic Frameworks: Controlling the Oxidation State of Cerium in One-Pot Synthesis Approach, *Adv. Funct. Mater.*, 2021, **31**(29), 2102582, DOI: 10.1002/adfm.202102582.

130 C. Simms, A. Mullaliu, E. T. Sarson, A. Solé-Daura, J. Puiggalí-Jou, J. J. Carbó, G. Aquilanti and T. N. Parac-Vogt, Tuning Oxygen Occupancy within Metal-Oxo Clusters for Enhancing Catalytic Activity of Zr-MOFs, *ACS Catal.*, 2025, **15**(16), 14279–14292, DOI: 10.1021/acscatal.5c03570.

131 L. Valenzano, B. Civalleri, S. Chavan, S. Bordiga, M. H. Nilsen, S. Jakobsen, K. P. Lillerud and C. Lamberti, Disclosing the Complex Structure of UiO-66 Metal Organic Framework: A Synergic Combination of Experiment and Theory, *Chem. Mater.*, 2011, **23**(7), 1700–1718, DOI: 10.1021/cm1022882.

132 M. Dan-Hardi, C. Serre, T. Frot, L. Rozes, G. Maurin, C. Sanchez and G. Férey, A New Photoactive Crystalline Highly Porous Titanium(IV) Dicarboxylate, *J. Am. Chem. Soc.*, 2009, **131**(31), 10857–10859, DOI: 10.1021/ja903726m.

133 Y. Fu, D. Sun, Y. Chen, R. Huang, Z. Ding, X. Fu and Z. Li, An Amine-Functionalized Titanium Metal–Organic

Framework Photocatalyst with Visible-Light-Induced Activity for CO2 Reduction, *Angew. Chem., Int. Ed.*, 2012, **51**(14), 3364–3367, DOI: 10.1002/anie.201108357.

134 C. H. Hendon, D. Tiana, M. Fontecave, C. Sanchez, L. D′ arras, C. Sassoye, L. Rozes, C. Mellot-Draznieks and A. Walsh, Engineering the Optical Response of the Titanium-MIL-125 Metal–Organic Framework through Ligand Functionalization, *J. Am. Chem. Soc.*, 2013, **135**(30), 10942–10945, DOI: 10.1021/ja405350u.

135 Y. Fu, H. Yang, R. Du, G. Tu, C. Xu, F. Zhang, M. Fan and W. Zhu, Enhanced Photocatalytic CO2 Reduction over Co-Doped NH2-MIL-125(Ti) under Visible Light, *RSC Adv.*, 2017, **7**(68), 42819–42825, DOI: 10.1039/C7RA06324E.

136 D. Ao, J. Zhang and H. Liu, Visible-Light-Driven Photocatalytic Degradation of Pollutants over Cu-Doped NH2-MIL-125(Ti), *J. Photochem. Photobiol., C*, 2018, **364**, 524–533, DOI: 10.1016/j.jphotochem.2018.06.044.

137 H.-T. Nguyen Thi, K.-N. Tran Thi, N. B. Hoang, B. T. Tran, T. S. Do, C. S. Phung and K.-O. Nguyen Thi, Enhanced Degradation of Rhodamine B by Metallic Organic Frameworks Based on NH2-MIL-125(Ti) under Visible Light, *Materials*, 2021, **14**(24), 7741.

138 Z. Wang, Z. Wang, Y. Pang, X. Wang and Y. Chen, Effect of Metal Substitution on the Optical Band Gap of MIL-125-NH2, *ChemistrySelect*, 2023, **8**(44), e202301509, DOI: 10.1002/slct.202301509.

139 L. Hanna, C. L. Long, X. Zhang and J. V. Lockard, Heterometal Incorporation in NH2-MIL-125(Ti) and Its Participation in the Photoinduced Charge-Separated Excited State, *Chem. Commun.*, 2020, **56**(78), 11597–11600, DOI: 10.1039/D0CC05339B.

140 C. L. Long, X. Zhang and J. V. Lockard, Pushing the Heterometal Doping Limit While Preserving Long-Lived Charge Separation in a Ti-Based MOF Photocatalyst, *J. Chem. Phys.*, 2023, **159**(19), 194704, DOI: 10.1063/5.0174664.

141 C. Serre, J. A. Groves, P. Lightfoot, A. M. Z. Slawin, P. A. Wright, N. Stock, T. Bein, M. Haouas, F. Taulelle and G. Férey, Synthesis, Structure and Properties of Related Microporous N,N′-Piperazinebismethylenephosphonates of Aluminum and Titanium, *Chem. Mater.*, 2006, **18**(6), 1451–1457, DOI: 10.1021/cm052149l.

142 M. Taddei, F. Costantino and R. Vivani, Synthesis and Crystal Structure from X-Ray Powder Diffraction Data of Two Zirconium Diphosphonates Containing Piperazine Groups, *Inorg. Chem.*, 2010, **49**(20), 9664–9670, DOI: 10.1021/ic1014048.

143 T. M. Reichenau, F. Steinke, M. T. Wharmby, C. Näther, T. A. Engesser and N. Stock, Targeted Synthesis of a Highly Stable Aluminium Phosphonate Metal–Organic Framework Showing Reversible HCl Adsorption, *Angew. Chem.*, 2023, **135**(26), e202303561, DOI: 10.1002/ange.202303561.

144 V. L. John, B. J. B, N. V. Kosova, S. M. B and R. Vedarajan, Revisiting Lithium Aluminium Titanium Phosphate Chemistry: Unveiling Advancements for All-Solid-State Batteries, *Next Mater.*, 2025, **8**, 100768, DOI: 10.1016/j.nxmate.2025.100768.

145 Y. Deng, C. Eames, L. H. B. Nguyen, O. Pecher, K. J. Griffith, M. Courty, B. Fleutot, J.-N. Chotard, C. P. Grey, M. S. Islam and C. Masquelier, Crystal Structures, Local Atomic Environments, and Ion Diffusion Mechanisms of Scandium-Substituted Sodium Superionic Conductor (NASICON) Solid Electrolytes, *Chem. Mater.*, 2018, **30**(8), 2618–2630, DOI: 10.1021/acs.chemmater.7b05237.

146 X. Li, H. Bian, W. Huang, B. Yan, X. Wang and B. Zhu, A review on anion-pillared metal–organic frameworks (APMOFs) and their composites with the balance of adsorption capacity and separation selectivity for efficient gas separation,, *Coord. Chem. Rev.*, 2022, **470**, 214714, DOI: 10.1016/j.ccr.2022.214714.

